CRACK FORMATION, ARREST AND PROPAGATION IN CONCRETE SLABS REINFORCED WITH CLOSELY SPACED STEEL WIRES

by

Hugh Enos Crow

B.S. United States Naval Academy

(1960)

Submitted in Partial Fulfillment

of the Requirements for the

Degree of Master of

Science

at the

MASSACHUSETTS INSTITUTE OF

TECHNOLOGY

May 23, 1969

Signature of Author.....
Department of Naval Architecture and Marine Engineering

Certified by.....
Thesis Supervisor

Approved by.....
Departmental Reader

Accepted by.....
Chairman, Departmental Committee
on Graduate Students

ABSTRACT

Crack Formation, Arrest and Propagation in Concrete Slabs Reinforced with Closely Spaced Steel Wires.

Hugh E. Crow

Submitted to the Department of Naval Architecture and Marine Engineering on May 23, 1969 in partial fulfillment of the requirement for the degree of Master of Science in Naval Architecture and Marine Engineering.

A technique is developed for the microscopic study of crack initiation, propagation and arrest in Ferro-cement specimens while they are being loaded in tension.

Test specimens were prepared with 33 gauge cold drawn music wire, 33 gauge soft stainless steel wire and 30 gauge galvanized iron flower wire in both parallel continuous wire and chopped random fiber configurations in steel percentages ranging from 0.75 to 2.7% by volume. Using these wire types one series of rich (0.7 cement/sand) mortar and one series of lean (0.4 cement/sand) mortar specimens were prepared and tested.

A large number of micro-photographs were taken to document the results of the observations. Positive verification of the crack arrest function of closely spaced wire reinforcement of concrete was obtained. Preferred crack propagation paths were observed to be through those regions having the lowest elastic modulus.

Thesis Supervisor: Fred Moavenzadeh
Title: Associate Professor of Civil Engineering

TABLE OF CONTENTS

Page

I. INTRODUCTION

Great interest has recently been focused on Ferro-cement as a marine construction material. Dr. P. L. Nervi, the inventor of Ferro-cement, deliberately fostered the amateur exploitation of this material for marine construction by patenting it only for architectural applications. (1) As a result, in the period from 1942 to the early 1960's most of the progress with ferro-cement was achieved by the trial and error efforts of amateur boat builders. Without really realizing what they were doing, all of the successful boat builders had formed a true "two phase" material not unlike fiberglass.

A "two phase" material is defined as one in which each phase contributes to the strength characteristics of the other so that the overall strength characteristics of the composite are greater than those of either phase taken by itself. (2) In the case of ferro-cement the cement mortar is found to be the load bearing fraction during short time loadings and the steel simply prevents the initiation or propagation of cracks, whereas for long time static loads the steel is the load bearing fraction.

1.1 Engineering Properties

Beginning with the 1960's much work has been done to

determine the engineering properties of concrete and ferro-cement. It was the extension of fracture mechanics to concrete in 1961 which helped to focus the attention of the materials engineers on ferro-cement. (3) Since that time, much progress has been made in determining the engineering properties of ferro-cement. Collins and Claman (4) have compiled an excellent state of the art summary of currently available engineering properties.

1.2 Concrete Cracking and Failure

Microscopic studies of concrete microcracking together with the application of Griffith Fracture Mechanics have firmly established that concrete failure is always linked with cracking of some sort. Recently there has been great emphasis on research into the causes, mechanisms and control of cracking in concrete. (5)

Moavenzadeh et. al. (6) developed a technique for straining plain concrete specimens while observing them with a microscope. Using this technique they were able to observe the initiation and coalescence of microcracks into the main throughgoing crack. This enabled them to establish the preferred initiation sites and the preferred propagation paths for cracks in concrete.

The success of these microscopy techniques with plain concrete suggests that similar techniques might be applied

to ferro-cement which heretofore has been studied on the macroscopic level. It is the purpose of this thesis to develop a similar technique for straining ferro-cement samples in tension while observing them with a microscope. Continued microscopic studies of fracture faces and strained sections will establish some factual data on the causes and mechanisms of crack initiation, propagation and arrest. These results will be compared and correlated with existing theory.

II. THEORY

2.1 General Considerations of the Strength of Concrete

Concrete is a mixture of cement paste, aggregate, and reinforcing material, if any. The strength of concrete then is a function of the strength of the paste, the aggregate, the reinforcing material and the bond between the paste and the other constituents. For these initial considerations, we will devote our attention to the cement paste since it is the most important constituent.

2.11 The Origin of Strength of Portland Cement Paste

Calcium silicate hydrate, commonly called tobermorite gel, is the constituent of hydrated portland cement which imparts strength to the hardened cement paste. The tobermorite gel derives its strength from two properties: the large surface area per unit weight of the colloidal gel particles and the large adhesive force per unit surface area of gel. (7)

The large surface area, about 1000 times the surface area of unhydrated cement particles results from the submicroscopic size of the tobermorite gel particles which have been postulated to be crystallite splines having a random distribution. (8) These submicroscopic colloidal particles are nevertheless large by atomic dimensions with the result that

few primary chemical bonds can form between colloidal particles. The principal source of adhesive force is from the inter particle magnetic attraction or van der Waal's bonds, and covalent chemical bonding exists only sufficient to maintain stability during water penetration. (9)

2.12 Porosity

Since tobermorite gel is the major constituent which contributes to the strength of pure portland cement paste, it follows that the strength of hardened paste is determined primarily by the concentration per unit volume of tobermorite gel. This concentration will be reduced by voids, uncombined water and entrapped air. Thus too large a w/c ratio as well as entrapped air can reduce strength of hardened paste.

2.13 Compressive Strength versus Tensile Strength

It is not yet clearly understood why the compressive strength is a full order of magnitude greater than the tensile strength of portland cement. It has been postulated that the difference derives from the random orientation of spline shaped gel crystallites. (8) When the gel is placed under tensile loading these splines can slide over one another with relatively few splines being broken even if deformation is large; whereas under compressive loading nearly all splines would ultimately be broken if the deformation were large.

2.14 Cracking and Fracture

Portland cement paste is a relatively brittle material and yet it displays almost ductile behavior as a result of microcracking. (10,11) Fracture occurs when the cracks join up and propagate completely through the material. To better understand this mechanism, we must review the evolution of fracture mechanics.

2.2 Evolution of Fracture Mechanics

The various fracture mechanics theories all start with the assumption of an initial flaw such as that treated by Inglis. (12) The flaw is assumed to be an elliptical hole in an infinite sheet with stresses being imposed at the external boundaries of the sheet.

2.21 Griffith Theory

Griffith conceived of fracture as being an energy transformation process in which a body of brittle material containing an initial flaw would pass from an unruptured condition of higher potential energy to a ruptured condition of lower potential energy. (13)

He assumed that the initial defect was a line crack of length 2C and defined three contributions to the total energy of the body. (U_T). "Elastic Strain Energy" (U): Potential energy arising from the work done on the system by the imposed stresses. "Surface Energy" (T): Energy required

for the formation of the new fracture surfaces as the original defect increases in size. "Internal Energy (I): Energy due to molecular motion.

Griffith calculated the decrease in Strain Energy per unit thickness due to formation of a crack of length 2C to be

$$U = \frac{\pi C^2 \sigma^2}{E}$$

and the increase in surface energy of the system due to the formation of a crack of length 2C is

$$T = 4C\gamma'$$

where $4C$ is the increase in surface area for a unit thickness and γ'. The Specific Surface Energy is defined as the energy required for formation of a unit area of fracture surface. Putting this together and taking the partial derivative with respect to C, we know that neither total energy nor internal energy change with crack length so:

$$U_T = U_I + U + T$$

and

$$0 = 0 + \frac{\partial U}{\partial C} + \frac{\partial T}{\partial C}$$

We see that $\frac{\partial T}{\partial C}$ is the energy dissipation rate due to crack extension and $\frac{\partial U}{\partial C}$ is the potential energy release rate due to crack extension.

Griffith showed that at $\frac{\partial U}{\partial C} \geq \frac{\partial T}{\partial C}$ the system becomes unstable and the crack propagates by a process which feeds upon itself since there continues to be more than enough potential energy

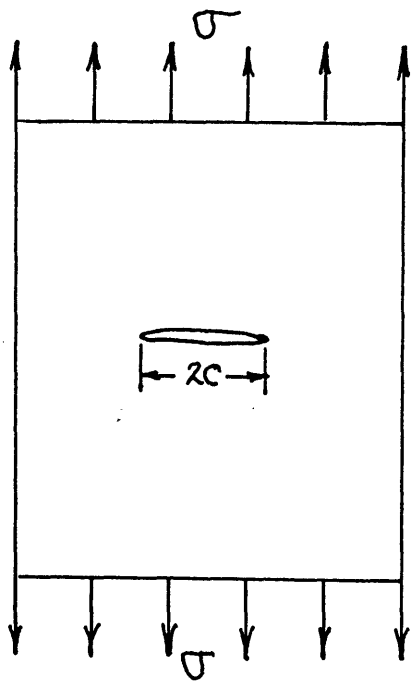

Figure 1. Griffith Theory Based on Initial Flaw.

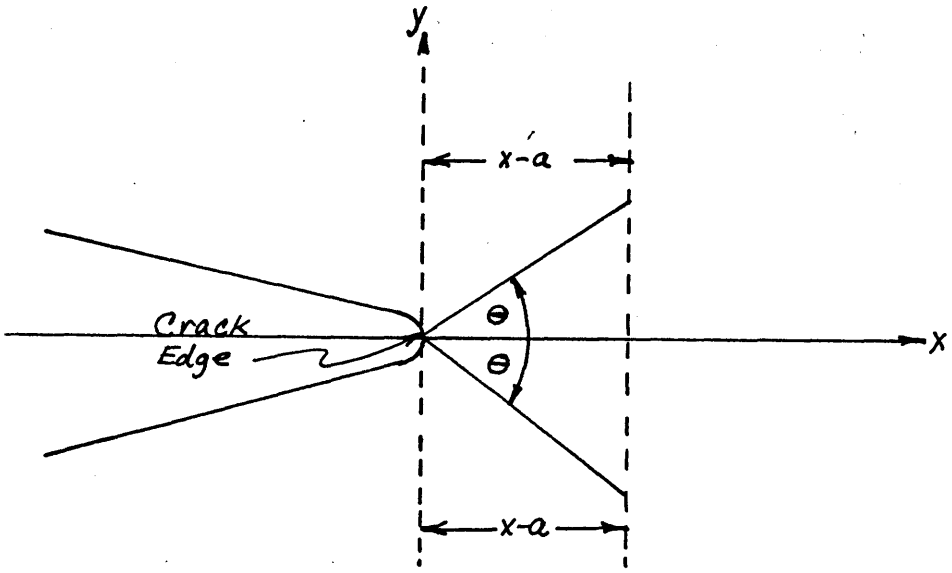

Figure 2. Crack Edge and Coordinates for Irwin Theory.

released to satisfy the energy dissipation due to formation of raw crack surface. In fact, in an ideal elastic material crack propagation approaches the speed of sound.

Substituting the expressions for U and T from above we find

$$0 = 0 + \frac{2\pi C \sigma^2}{E} + 4\gamma$$

Then define this stress at $\frac{\partial U}{\partial C} \geq \frac{\partial T}{\partial C}$ as σ_C and solve:

$\sigma_C = \sqrt{\frac{2E\gamma}{\pi}}$ for plane stress.

Sack (8) extended Griffiths theory to three dimensions and showed that if plane circular cracks of radius C are distributed in a brittle solid, rupture will be determined solely by the maximum tensile stress σ and will be unaffected by smaller tensile (and within limits compressive) stresses at right angles to it. Rupture occurs if

$$\sigma \geq \sigma_C = \sqrt{\frac{2E\gamma}{\pi C (1-\mu^2)}}$$

2.22 Irwin Theory

Because of much evidence of ductile behavior at the tip of flaws, Irwin (15, 16) was prompted to adopt a different approach to the Inglis flaw hypothesis. He assumed a line crack of zero thickness but considered the stress field in the immediate vicinity of the flaw tip rather than assuming the stress field to be uniform as did Griffith. Using the coordinate system illustrated in figure 2, he derived the stresses

parallel and normal to the crack as follows:

$$\sigma_y = \sqrt{\frac{EG}{2\pi r}} \cos\frac{\theta}{2}\left(1 + \sin\frac{\theta}{2}\sin\frac{3\theta}{2}\right)$$

$$\sigma_x = \sqrt{\frac{EG}{2\pi r}} \cos\frac{\theta}{2}\left(1 - \sin\frac{\theta}{2}\sin\frac{3\theta}{2}\right)$$

where r is radius from crack tip to point where σ is being considered and θ is the angle between r and the x axis. The parameter G is seen to be independent of r and θ and Irwin showed it to be the magnitude of the energy exchange associated with unit extension of the crack. In other words it is the same as $\frac{\partial U}{\partial C}$ from the Griffith Theory.

This G may be considered to be the force tending to cause crack extension but it is most often called"Strain Energy Release Rate".

Another factor K called "Stress Intensity Factor" is defined such that

$$G = \frac{\partial U}{\partial C} = \frac{\pi K^2}{E}$$

At the condition $G = \frac{\partial U}{\partial C} \geqslant \frac{\partial T}{\partial C}$, define $G = G_c$ called "Critical Strain Energy Release Rate" or "Fracture Toughness Modulus" and $K = K_c$ called "Critical Stress Intensity Factor". These are found to be fundamental physical characteristics of a given material just as are Young's Modulus, E or Poissons Ratio, μ.

2.23 Orowan Derivation

Orowan also started with the elliptical Inglis model of

an initial flaw. Inglis (12) showed that the stress concentration due to a flaw is given by

$$S = 2\sigma\sqrt{c/\rho}$$

where: S = Stress Concentration
σ = Applied Stress
C = $\frac{1}{2}$ Crack Length
ρ = Radius of Curvature of Crack Tip

Since in actuality in a brittle material, the radius of curvature of the crack tip, ρ is of the same order of magnitude as the interatomic spacing, a

$$S = 2\sigma\sqrt{c/a}$$

Orowan (17) then calculated the molecular cohesion at the crack tip to be of the order of magnitude of

$$\sigma_m \approx \sqrt{\frac{2E\gamma}{a}}$$

If the stress concentration is critical, $\sigma_m = S_c = 2\sigma\sqrt{c/a}$ and $\sigma = \sqrt{\frac{\gamma E}{2c}}$ for fracture. Recall from Griffith Theory, $\sigma = \sqrt{\frac{2\gamma E}{\pi c}}$ for fracture. So Orowan's derivation verifies the Griffith and Irwin derivations within the accuracy of the assumptions made by Griffith and Irwin.

2.24 Extension to Non Brittle Materials

The Griffith theory has been modified and extended to materials which undergo considerable plastic deformation prior to the initiation of unstable crack propagation (18, 19). Felbeck and Orowan (19) modified the Griffith Equation to become:

$$\sigma = \sqrt{\frac{2E(\gamma + W_p)}{\pi c}}$$

where W_p is the plastic work term accounting for the dissipation of strain energy in plastic deformation. The energy absorption term T now may be expressed: $T = 4C\ (\gamma + W_p)$ at room temperature for low carbon steels and similar ductile metals, the plastic work term, W_p, is orders of magnitude greater than the surface energy term γ. This modified Griffith criterion is applicable only to essentially brittle fractures, however, where the plastic deformation is confined to a thin layer at the walls of the crack while the bulk of the material is purely elastic (17).

Application of the Energy criterion $\frac{dU}{dc} \geqslant \frac{dT}{dc}$ fails, however, when the fracture is essentially ductile(20). It can be seen that since the fracture is essentially ductile, it is independent of the elastic modulus; E may be taken as infinite so that dT vanishes. In this case, then the Griffith energy criterion fails. Orowan (20) showed that such unstable ductile fracture can take place only if a region of elastic material lies outside the region of plastic faulure. The resulting system may be modeled by a spring in series with the plastic material and high velocity ductile fracture occurs if $\frac{\partial^2 U}{\partial c^2} \geqslant \frac{\partial^2 T}{\partial c^2}$.

2.25 Crack Arrest

We have seen that once a crack is initiated in a homogenous medium and the condition $\frac{\partial U}{\partial c} \geqslant \frac{\partial T}{\partial c}$ remains, no further energy

need be added to the system for crack propagation to continue. It follows, however, that anything which causes a significant increase in the energy absorption term T, could cause a reversal of the energy relationship so that:

$$\frac{\partial U}{\partial c} < \frac{\partial T}{\partial c}$$

Crack propagation should be stopped or "Arrested" in such a case.

Recall that the general energy absorption term is now expressed: $T = 4c\ (\gamma + Wp)$.
Thus any inhomogeneity which significantly increases γ or Wp can cause crack arrest.

By treating Wp for steels as a function of temperature, alloy content, and heat treatment, Pellini (21) has developed empirical design criteria which allow the ship designer to take full advantage of this crack arrest mechanism. We will see that crack arrest may be achieved by somewhat different mechanisms in concrete.

2.3 Application of Fracture Mechanics to Concrete

Kaplan (22) suggested that the Griffith theory might be extended to concrete even though concrete is a heterogeneous composite on a macroscopic scale whereas the Griffith theory assumes a homogeneous material on a microscopic scale. He assumed that the effective values of Youngs Modulus, E, and Poissons Ratio, μ, for the composite was a weighted average

of the values for the constituents. He then used the Griffith Equation modified for beam flexure

$$G = \frac{(1-\mu^2)\sigma_n{}^2(d-c)}{E} \cdot f\left(\frac{c}{d}\right)$$

to calculate G_c where μ = Poissons Ratio, σ_n = notch stress, d = beam depth, c = notch depth and $f(\frac{c}{d})$ is a factor developed by Winne and Wundt (23) to account for the relative size of the notch. In this case $f\ (c/d) = \frac{\pi c}{d}(1 - \frac{c}{d})^3$ These theoretical calculations agreed closely enough with experimental determinations of G_c to verify that Griffith Fracture Mechanics could be modified and extended to concrete. Kaplan's results indicated that the energy requirement for propagation in cement paste was an order of magnitude larger than the surface energy of the nominal new crack surface. Glucklick (24) suggested that this increased energy requirement was due to the actual formation of much larger actual fracture surface than the nominal cross sectional area. For cement paste he suggested that this additional crack surface takes the form of microcracks near the crack tip. Hsu et. al. (25), Moavenzadeh et. al. (26) and others have verified by direct microscopic observation, that this is true. In Kaplan's work the value for γ was assumed to be surface free energy which ignored the possibility of plastic flaw and microcracking at the crack tip. Moavenzadeh et. al. (26) used a method for finding the effective γ which had been proposed by Nakayama(28)

for stable or semistable fractures: $U = 2A\gamma$

where U = measured input energy, A = fractured surface area (effective cross sectional area), γ = surface energy per unit area.

γ computed from this formula includes all the thermodynamic surface energy as well as any energy dissipated in plastic deformation so is an Effective Specific Surface Energy.

In paste, the fracture surface tends to be relatively straight across the stress field. In mortar and concrete with larger aggregate, however, the crack path is quite circuitous and meanders around sand and aggregate particles.

2.32 Aggregates in Plain Concrete

Lott and Kesler (28) have explained this characteristic meandering path of cracks in concrete in terms of the crack arrest mechanism. In most aggregates, the surface energy is higher than in the cement paste so that if a crack attempts to penetrate an aggregate particle the energy demand is suddenly greatly increased. The crack tends to follow the path of least resistance and passes around the aggregate. This, of course, increases the surface area so places an additional drain on the elastic strain energy supply. We recall that crack arrest occurs if sufficient drain on the energy supply is present to cause $\frac{\partial U}{\partial c} < \frac{\partial T}{\partial c}$. This tendency to cause arrest increases if the modulus of elasticity of the aggregate is increased relative to that of the paste matrix,

if the aggregate size is increased and if the tensile bond strength of the paste aggregate interface is increased. Lott and Kesler (28) defined a Pseudo Fracture Toughness

$$K_c' = K_{pc} + f(arr).$$

where K_{pc} = Critical Stress Intensity Factor of the cement paste matrix dependent upon w/c ratio, curing time, temperature, etc.

f(arr) = A complex arresting function dependent upon the factors listed above.

Defining K_c' and working with it focuses attention upon the importance of these variables but no one has yet been able to separate K_{pc} from f(arr) so that one must still assume a homogeneous medium with the engineering properties resulting from weighted averages of the constituent properties.

2.33 Inelastic Behavior of Plain Concrete

Much work has been done in establishing that the nonlinear stress strain curve for concrete is related to microcracking. Figure 3 taken from Moavenzadeh et. al. (26) presents a good summary of this relationship. Region A corresponds to the nearly linear portion of the stress strain curve in which only a small amount of creep occurs and most of the deformation is recoverable. As the load is increased through Region B, the bond cracks increase in length, width and number and the stress - strain curve begins to depart appreciably from a straight line. In Region C, at about 70% of the ultimate load,

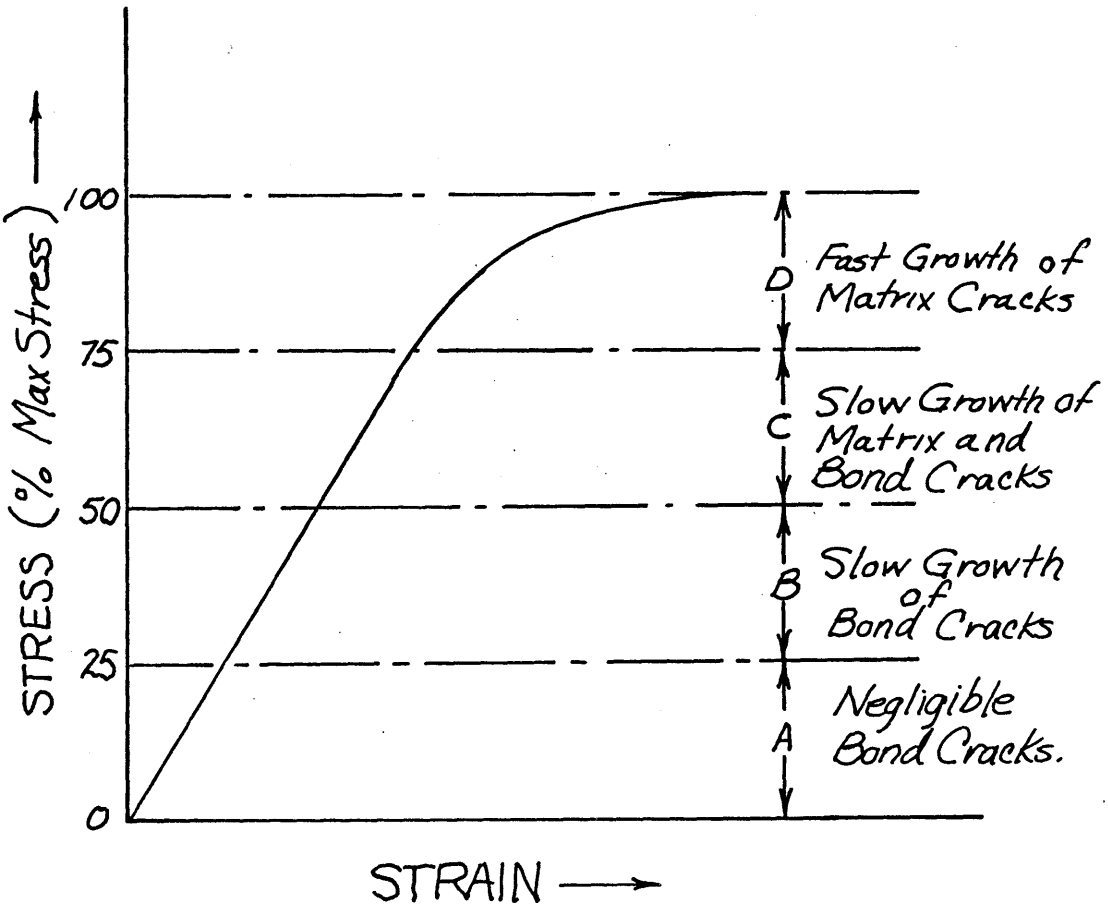

Figure 3. Diagrammatic Stress-Strain Curve.

the number of cracks through the mortar increases appreciably and begin to join up through bond crack bridges to form continuous cracks.

Region D still represents considerable load carrying capacity because once a continuous microcrack has formed across a region another region picks up the load until it develops a continuous microcrack. This process continues in a highly redundant manner until extensive crack patterns are formed at the ultimate load carrying capacity at which point the stress strain curve begins to descend.

It has been established that this inelastic behavior is due to the heterogeneity introduced by the aggregates. Hsu and Slate (29) have established that the tensile bond strength of the paste-aggregate interface varies from 41 to 91 percent of the paste tensile strength depending upon the aggregate rock type and the water-cement ratio. Further, the paste aggregate interface bond strength decreases with increasing size of aggregate.

Shah and Winter (30) have developed a mathematical model which predicts stress-strain curves which closely resemble the actual curves. Their theory is based upon the structural unit illustrated in Figure 4. This unit assumes a single piece of circular cylindrical aggregate embedded in a prism of mortar.

It is assumed that a given cross section of a concrete specimen under uniaxial compression is made up of n structural

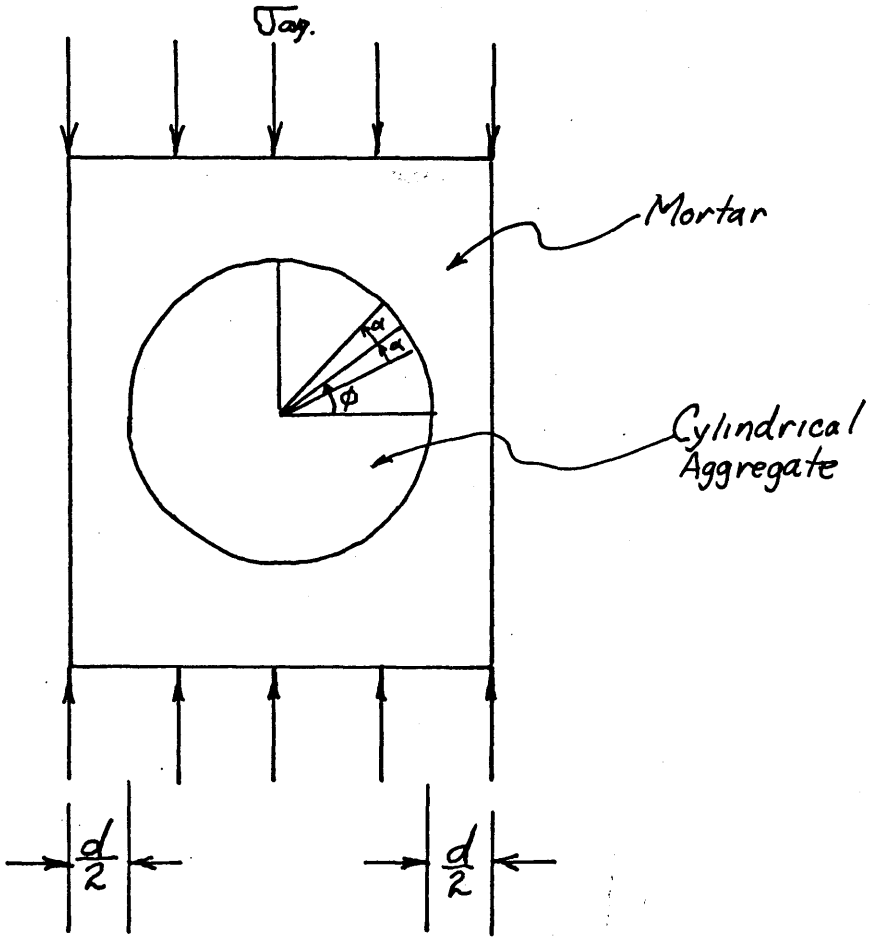

Figure 4. Structural Unit for Mathematical Model.

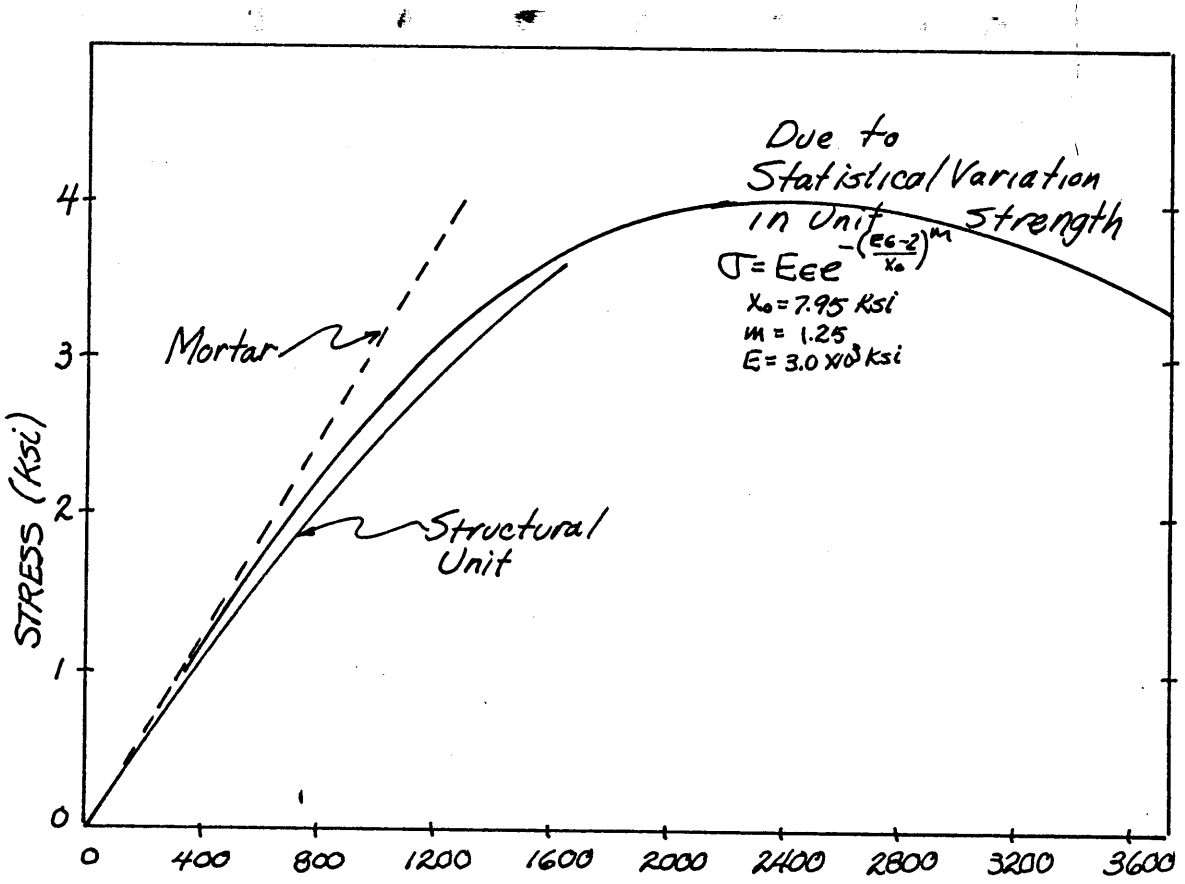

Figure 5. Stress-Strain Curve Predicted by Mathematical Model.

units. The ultimate strengths of these units are assumed to be distributed according to a distribution function G(x), which is the probability that the strength of a unit has a value greater than or equal to x ksi. This G(x) is an unknown which must be related to the experimentally determined distribution of compressive strengths of whole specimens.

Assume: 1) The strength of each unit is independent of others, 2) Hookes law is valid for each unit and all units have the same modulus of elasticity, 3) Plane sections remain plane, 4) As soon as the ultimate strength of one unit is exceeded it's load bearing capacity closes and that stress is uniformly distributed to other units not having exceeded ultimate strength.

A normal distribution was taken for the strengths of the concrete cylinders and a Weibull type distribution function was assumed: $G(x) = e^{-(\frac{x-x_1}{x_o})^m}$ where x_1 is the lowest possible structural unit and x_o and m are constants depending upon the mean and variation of the cross section ultimate strength.

$$\sigma_{avg} = x\, G(x) = x\, e^{-(\frac{x-x_1}{x_o})^m}$$

$$\epsilon = \frac{x}{E}$$

Figure 5 shows one Stress Strain Curve plotted from this relation.

2.34 Failure of Concrete

We have seen that concrete retains considerable load carrying capacity even after continuous crack patterns form.

This stable crack propagation is due to the heterogeneous composition of the concrete which permits the excess strain energy to be released without the catastrophic propagation of a self feeding crack which is characteristic of a homogeneous brittle material.

Failure of concrete is normally defined as the condition when the paste-aggregate interface cracks begin to extend into the paste matrix. This crack propagation need not be cataclysmic nor even fast but must constitute failure since continued application of the stress at which this occurs will eventually cause complete disruption.

2.4 Ferro-Cement

2.41 Mathematical Model

Romualdi and Batson (3 and 31) have proved that it is possible to achieve true two phase action in reinforced concrete by using closely spaced steel wires. As a flaw in the concrete tends to enlarge to a crack, displacements develop in the material ahead of the crack as a result of the stress field singularity at the crack edge. The greater rigidity of the steel wires, however, opposes these displacements, and forces are exerted by the wires on the concrete matrix. The requirement for compatibility at the wire-matrix interface makes it possible to calculate these forces. They can be interpreted in fracture mechanics terms as being a reduction in the crack extension force, in other words, a crack arresting force. It is found (31)

that the stress required to extend a crack beyond the area enclosed by a bundle of wires is inversely proportional to the square root of the wire spacing.

The analytical model is shown in Figures 6 and 7. The application of a uniform remote tensile stress tends to cause additional displacements of the concrete in the neighborhood of the crack but these extensional strains are resisted by the wires which are assumed infinitely stiff. This resistance causes a distribution of shear forces along the wires which act to close the crack.

Solutions for the interaction force distribution are obtained for discrete points along the wire as shown in Figure 7. The points are spaced at intervals h, and assuming the distributed force along the wire at any point, y_j, to be constant over the interval h, the interaction force at any point y_j, is P_j, equal to $f_j h$. Let v_i be the y directed displacement of a discrete point, y_i, because of the presence of the crack if the wires were not present; and let d_{ij} be the displacement of the point y_i in the concrete due to a unit force at the wire at the location y_j. Neglect extensions of the wire since it is orders of magnitude stiffer. Then for compatibility to be satisfied, there must be no relative displacement between the wire and concrete at each of the n discrete points:

$$v_i - \sum_{j=1}^{n} d_{ij} P_j = 0$$

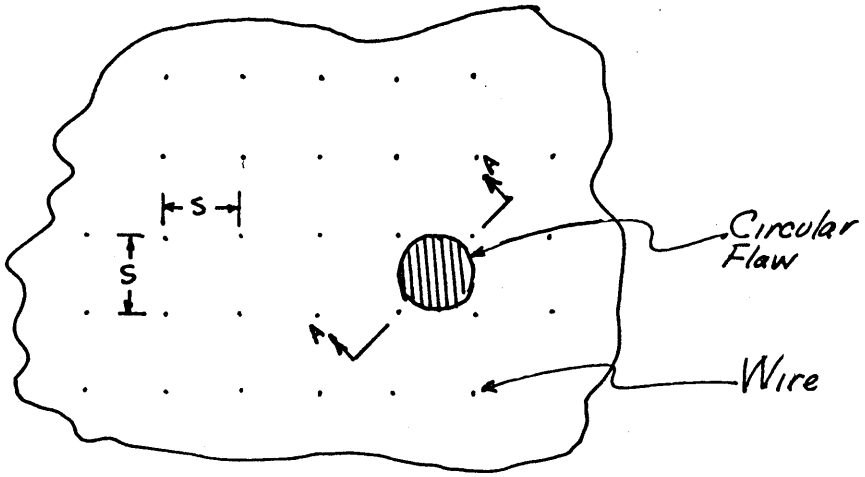

Figure 6. Cross Section Through Wire Reinforced Concrete at a Flaw.

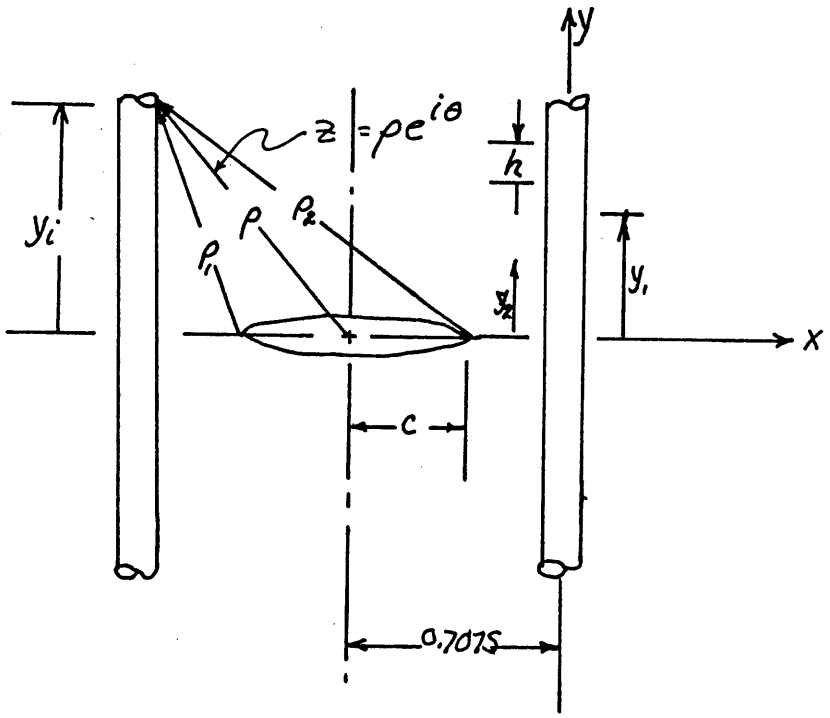

Figure 7. Section A-A of Figure 6 Showing Circular Crack Surrounded by a Bundle of Wires.

The displacement v_i is calculated with the aid of a stress function taken from Westergaard (32)

$\phi = R_e\ \bar{Z} + yI_m\ \bar{Z}$ in which $\bar{Z}$ is the complex variable $\bar{Z}(z) = \frac{z}{\sqrt{z^2+c^2}}$

The plain strain displacement is then given by

$$v = \frac{(1+\mu)}{E}\left[2(1+\mu)\ \mathrm{Im}\ \bar{Z} - y\ \mathrm{Re}\ \bar{Z}\right]$$

The displacement at y_i due to a unit load at y_j is

$$d_{ij} = \frac{1}{B}\left[\frac{(y_i + y_j)^2}{R_1^3} - \frac{(y_i-y_j)^2}{R_2^3} + \frac{Q+3G}{Q+G}\left(\frac{1}{R_1} + \frac{1}{R_2}\right)\right]$$

$$+ \frac{\bar{\sigma}\rho_1^{\frac{1}{2}}\rho_2^{\frac{1}{2}}(1+\mu)}{E}\left[2(1+\mu)\sin\left(\frac{\theta_1+\theta_2}{2}\right)\right.$$

$$\left.\frac{-y_i\rho}{\rho_1\rho_2}\cos\left(\theta - \frac{\theta_1+\theta_2}{2}\right)\right] - \frac{\bar{\sigma}y_i}{E}\left(1-\mu-2\mu^2\right)$$

where: r_2 = wire radius,

$$R_1^2 = r_2^2 + (y_i + y_j)^2\ ;\ R_2^2 = r_2^2 + (y_i-y_j)^2$$

$$Q = \frac{E}{(1+\mu)(1-2\mu)}\ ;\ G = \frac{E}{2(1+\mu)}$$

$$B = \frac{8\pi G\ (Q+2G)}{(Q+G)}$$

The set of simultaneous equations $v_i - \sum_{j=1}^{n} d_{ij}P_j = 0$ is then solved for P_j with the aid of a computer given any remote uniform stress σ.

The total Stress Intensity Factor, K_T, can be computed from the formula:

$$K_T = K_\sigma - K_p = \frac{2\sqrt{c}}{\pi}(\sigma - p)$$

where K_σ = Stress Intensity Factor due to the remote stress σ.

K_p = Stress Intensity Factor due to the forces P_j.

p = The distributed pressure on the area occupied by the crack due to the forces P_j on the wires adjacent to the crack.

This K_T is then compared with the Critical Stress Intensity Factor, K_c, to determine if the crack propagation due to the selected σ will be stable or unstable. Figure 8 illustrates the results of computer solutions from the above model. Theoretical results predicted by this model have been found to compare very favorably with experimental results.

2.42 Short Random Fibers as Reinforcement

The initial work done by Romualdi and Batson (3,31) was with continuous parallel wires but theoretical calculations of the bond stress distribution along the wires shown in Figure 9 indicated that the greatest bond shear stress on the wire occured very close to the crack and that at approximately ten times the wire spacing the bond stress was negligible (33). This suggested the use of short steel wire fibers of lengths at least ten times the effective wire spacing. Romualdi and Mandel (34) extended the mathematical

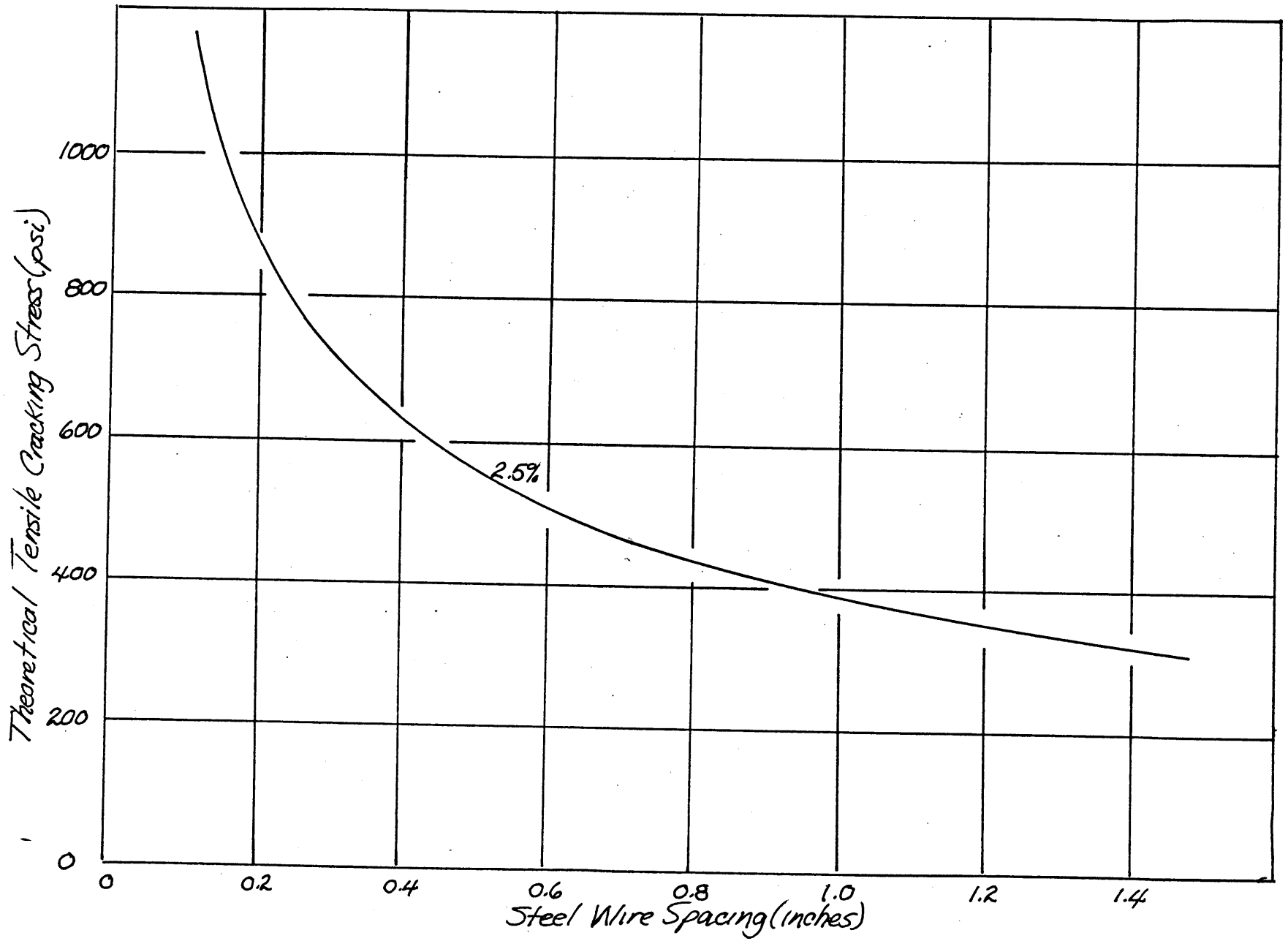

Figure 8. Theoretical Cracking Stress as a Function of Wire Spacing.

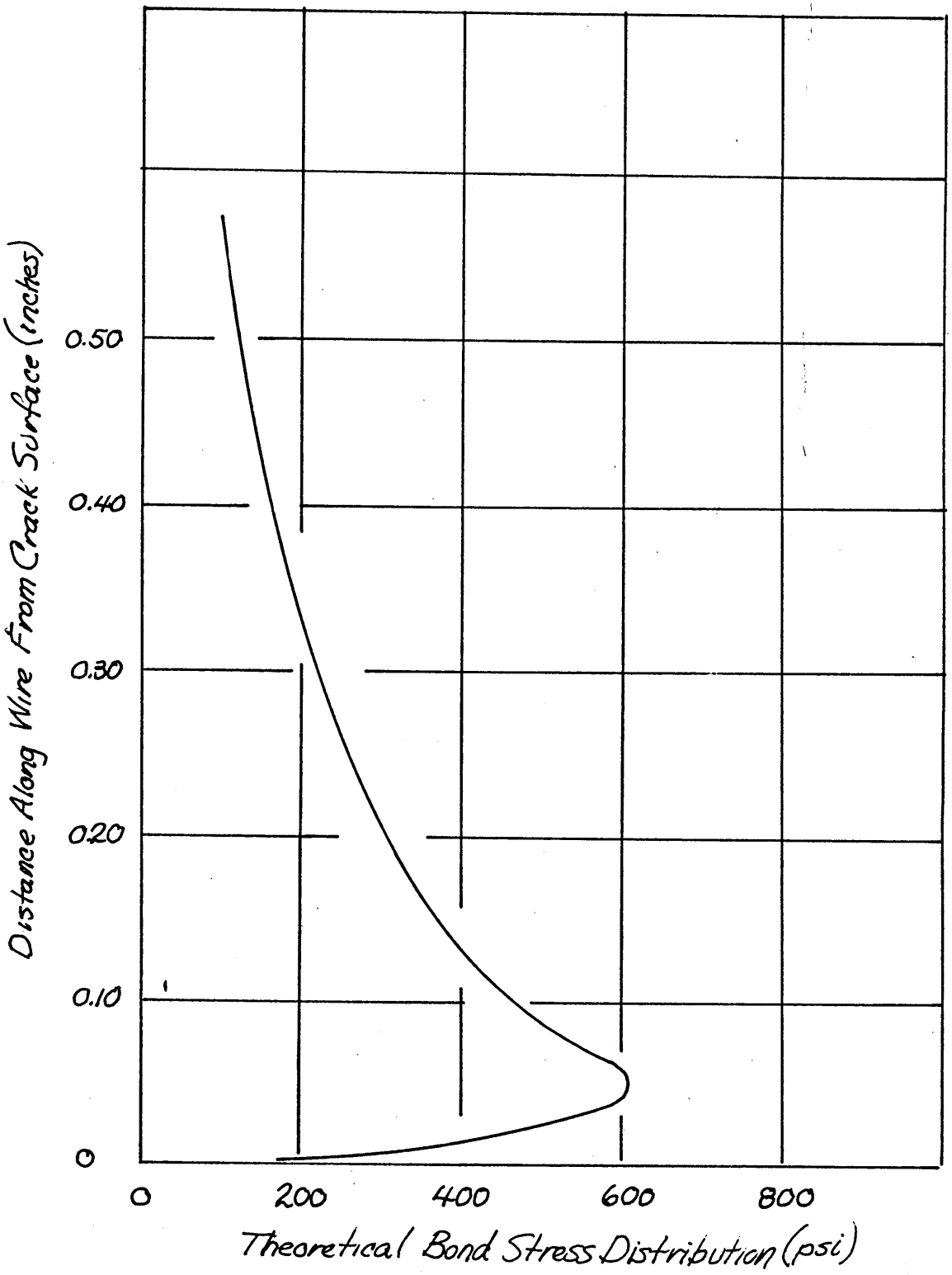

Figure 9. Theoretical Bond Stress Distribution

model to include these short fibers. Wires were assumed to be uniformly distributed but of random orientation. To be effective in arresting crack extension, wires must be parallel to the tensile stress field. Thus a statistical average length of the wire in the x direction is computed. See Figure 10 .

$$\frac{N \int_0^{\pi/2} \int_0^{\pi/2} L \cos\theta \cos\phi \, d\theta \, d\phi}{N (\pi/2)^2} = 0.41 \, L.$$

Only 41 percent of each wire's length is effective in crack arrest; hence only 41 percent of the steel volume is effective.

Let V = Total volume of reinforced concrete

N = Number of wires

Then the average effective spacing of the wire centroids is:

$$S_{ce} = \sqrt[3]{\frac{V}{0.41N}}$$

A certain amount of overlapping will occur since L will usually be larger than S_{ce}. The number of effective wires at a cross section is:

$$n_w = \left(\frac{1}{S_{ce}}\right)^2 \left(\frac{L}{S_{ce}}\right) = \frac{L}{S_{ce}^3}$$

The average spacing of the wires is:

$$S = \frac{1}{\sqrt{n_w}} = \sqrt{\frac{V}{0.41NL}}$$

Expressed in terms of wire diameter, d, and volume percentage steel, p, $S = 13.8d\sqrt{\frac{1}{p}}$

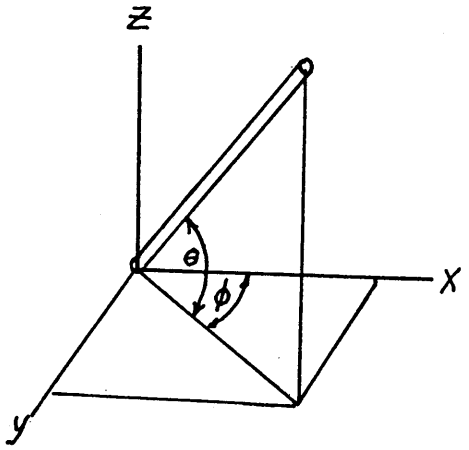

Figure 10. Wire of Length L in Random Orientation

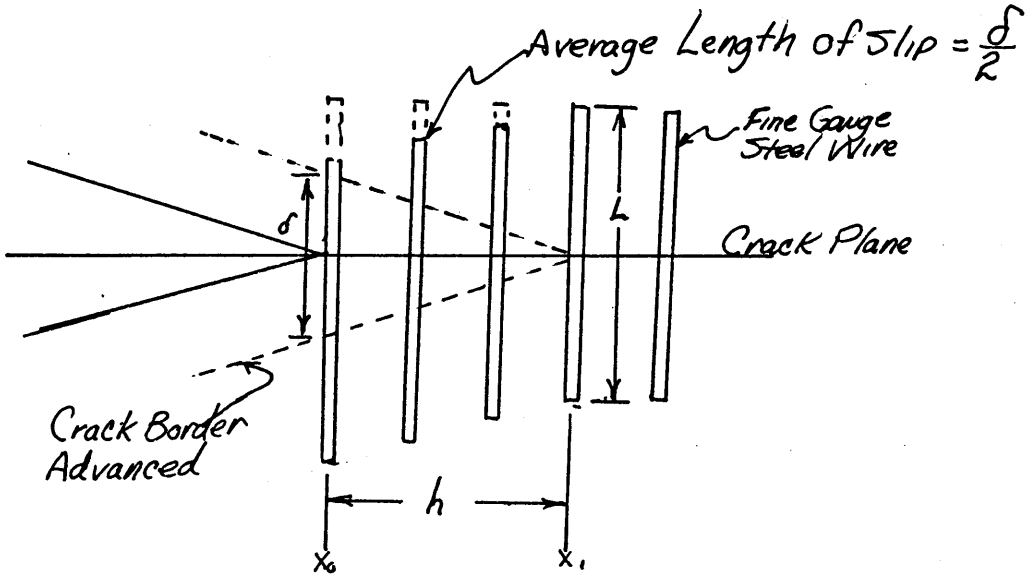

Figure 11. Idealized Version of Wire Fiber Slipping in Zone of New Crack Surface.

The model previously used assumed that crack growth would be contained within the boundaries of a given bundle of wires which really amounts to stopping the initiation of a running crack. Now consider that the crack front has passed some wires and is attempting to pass others (35). The toughness of wire reinforced concrete is a result of the energy required to strip the short wires free of their adhesion in advance of the crack front. Referring to Figure 11, assume a distribution of wires of length L and diameter d. As the crack front moves a distance h, new crack area 2 x 1 x h =2h (per unit depth) is formed. After traveling h distance, the average amount that the wires are stripped back is $\delta/2$. Stripping each of these wires constitutes irrecoverable work corresponding to W_p in the expression $T = W_p + \gamma$ and γ is negligible by comparison with W_p. Thus $G_c = Nf\,\delta/2$ is approximately the work associated with the formation of a unit area of crack surface where:

N = number of wires intersecting new crack surface.

f = stripping force per wire.

Let: $f = u\,(\pi d)\,(L/2)$

$$N = \frac{1}{S^2} \quad ; \alpha = \delta/h.$$

where u = bond strength

d = wire diameter

L = wire length.

S = Effective Spacing

α = Ratio of crack width to crack length.

then $G_c = \frac{u\pi d L\alpha}{4S^2}$

Now substitute $S = 13.8\ d\sqrt{1/p}$ to account for random orientation to get:

$$G_c = \frac{u\pi L\alpha p}{760d}$$

The magnitude of the bond strength u may be determined by experiment for a given wire and cement mix, and the other factors are dependent upon choice of wire size and percentage steel.

2.43 Yielding of Wire Reinforcement

If the wires are continuous or very long there is a possibility of the bond strength holding so that any opening of the crack at the wire must be associated with deformation of the wire.

The work associated with this crack movement has been shown (4) to be: $G_c = N\int_0^{\epsilon} \sigma\ a_w d$

where: σ = stress in wire

ϵ = strain in wire

a_w = area of each wire

N = number of wires encountered per unit crack extension.

Some irrecoverable work must be associated with this process. If the bond pulls out over some portion of the wire's length, frictional work will dissipate energy although the wire may not have yielded. If the wire does yield, then

of course, plastic work takes place. In either case, Fracture Toughness is increased.

2.44 Creep and Relaxation Effects

Heretofore, no mention has been made of the fact that the load carrying characteristics of concrete are very time dependent. If a constant tensile stress is applied to a ferro cement member, creep will eventually cause sufficient elongation of the concrete matrix to completely unload and place the entire load on the steel reinforcement. Similarly, application of a fixed strain to a ferro cement member will initially load the concrete but relaxation of the concrete will eventually shift the load to the steel reinforcement.

III. PROCEDURE

3.1 Materials Tested

Two mortar mixes were used in order to compare the qualities of an economical cement-sand ratio with those of the rich cement-sand ratio used by Collins (36, 37). Both used Type I Portland Cement and fine graded silica sand (Ottawa C-109) with a fineness modulus of 1.72.

Lean mix: C/S ratio = 0.405,

W/C ratio = 0.46

Rich mix: C/S ratio = 0.7,

W/C ratio = 0.36

Two methods of controlling wire content were used in order to compare the qualities of continuous wire reinforcement with those of chopped wire reinforcement. The continuous wires were threaded through a plexiglass mold in layers of wires, wire spaced at uniform intervals of 0.08 inches, 0.10 inches and 0.12 inches in successive samples. These layers were then sliced out of the resulting beam with a diamond saw. The series of lean mix specimens included both single layers and double layers of wires but the rich mix series included only double layers. Chopped wire samples were prepared with 2 percent by volume of steel wires distributed with uniform spacing but random orientation in the mortar as it was cast in the plexiglass mold. Effective spacings were computed with the formula: $S = 13.8\ d\ \sqrt{1/p}$ as derived in paragraph 2.42.

Three types of wires were tested:

33 gauge Music Wire
(Y.S. = 190,000 psi.; U.T.S. = 330,000)

33 gauge Soft Stainless Steel
(Y.S. = 55,700 psi.; U.T.S. = 101,000)

30 gauge Galvanized "Flower Wire"
(Y.S. = 42,200 psi.; U.T.S. = 49,200)

The 30 gauge galvanized flower wire was tested because it was the only the fine gauge galvanized wire which was available locally when the delivery of 33 gauge galvanized steel wire and other wire types for previously programmed tests were delayed. Because of this delay, single layer specimens and 0.12 inch spacing specimens for the galvanized wire subseries and the rich mix subseries were deleted from the program.

3.2 Sample Preparation

3.21 Casting

Parallel wire samples were cast in the mold shown in Figure 12a. Wires were threaded through holes drilled in the end pieces at the desired spacing and attached by alligator clips to a spring with just enough tension to keep the wires from sagging. Mold dimensions were 1 inch deep by 1 inch wide by 12 inches long. The chopped wire samples were cast into box molds $\frac{1}{2}$ inch deep by $2\frac{1}{2}$ inches wide by 6 inches long. Wire was hand cut to 1 1/8 inch length fibers with diagonal wire cutters. Mortar was mixed with a heavy duty five quart food mixer. For those samples using

chopped wire, the wire fibers were added after the water had been thoroughly mixed. Care had to be exercised in order to keep the soft stainless and galvanized fibers from entangling and bunching up into balls instead of being uniformly mixed.

Mortar was vibrated and compacted using the vibrating table and pneumatic compacting tool shown in Figure 12b.

3.22 Curing

These beams were kept 24 hours in a 100% humidity moist room, then stripped from the molds and cured under water for seven days. The lean mix beams were then dried for seven days before slicing but the rich mix beams were kept under water for the full fourteen days prior to slicing up into specimens, in order to limit shrinkage cracking.

3.23 Slicing

A 0.030 inch thick precision diamond saw mounted on a hydraulic ram type shaper with automatic depth feed, was used to slice up the specimens. It was necessary to limit the depth of cut per pass to about 0.003 inches for the chopped wire samples and about 0.010 for the parallel wire samples in order to avoid heating and warping of the precision thin saw blade.

As a result, each slab took approximately an hour to slice out of the beam but the resulting surface required no additional polishing prior to study under the microscope.

Notches of 0.15 inch were then cut into one edge of the samples with the precision diamond saw. A heavier duty diamond saw was then used to cut the samples to length.

In order to provide a grip for the straining device, steel plates 1/16 in. X 3/8 in. X 1 in. were attached to each face of the specimen ends with Hysol Epoxy Patch Cement.

3.24 Pullout Specimens

In order to determine the efficiency of the bond between each mortar type and each wire type, two pullout specimens for each of the six combinations were prepared. Standard"dogbone" specimen molds were used to prepare plaster of paris wire holder shields. These were cut in half, drilled to receive the free end of the wire, and replaced in the mold with the wires in place. Mortar of the appropriate type was then cast into the empty half of the mold with 1 1/8 inches of wire extending into the mortar. These samples were then given the same curing cycle as already described for the test specimens.

3.31 Straining Device

In order to observe the specimens at the same time that they were being strained it was necessary to build a sturdy frame which would be essentially infinitely stiff in comparison to the concrete specimen and yet would be small enough so that it could be easily moved by the delicate

positioning screws of the microscope specimen table. The device finally used was modeled after a smaller frame used to strain plastic test specimens with the modifications of a load cell on one end and a micrometer screw on the other. (See Figure12c) The load cell consists of a yoke machined to a cross section of 1/16 in. X 1/2 in. to each side of which a Baldwin-Lima-Hamilton, SR-4 Type 107, strain gauge is bonded. The micrometer screw consists of a 1 inch diameter cylindrical rod which is drilled and tapped for 1/4-20 threads. Friction on the thrust bearing surface was reduced by machining a shallow cylindrical recess on the bearing end to leave an effective bearing surface of 0.25 square inches. A nut was machined on the outside edge of the cylinder so that it was relatively easy to hand turn this nut to exert up to 200 pounds tensile force on the specimen.

The edge of the cylindrical circumference was then calibrated to read in thousandths of an inch: 1 revolution = 0.036 inch. This micrometer screw could then be read from an index mark on the frame to the nearest 0.0005 inch of specimen elongation .

3.32 Strain Indicator

A Digital Strain Indicator, Model P-350 made by the Instruments Division of the Budd Company was used to read strain from the load cell. A full resistance bridge was

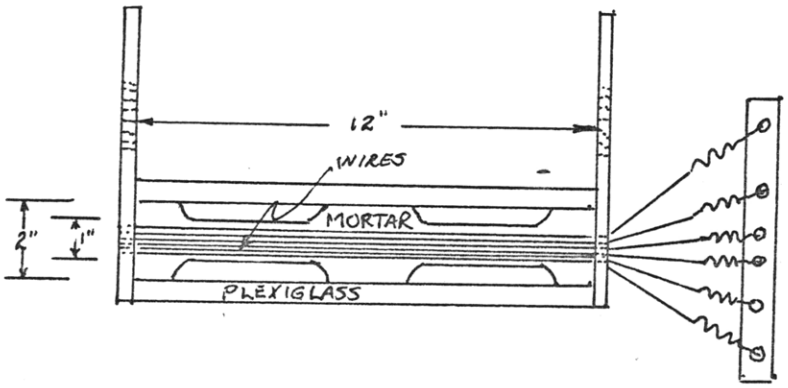

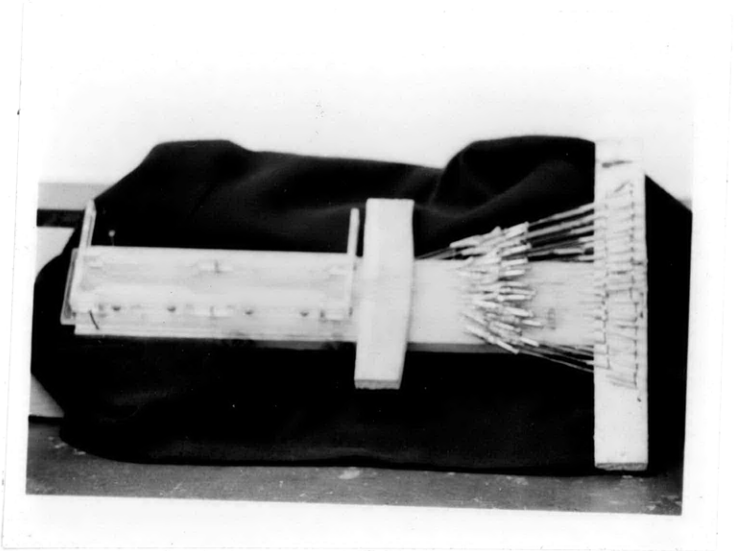

Figure 12a Parallel Wire Specimen Mold and Tension Frame.

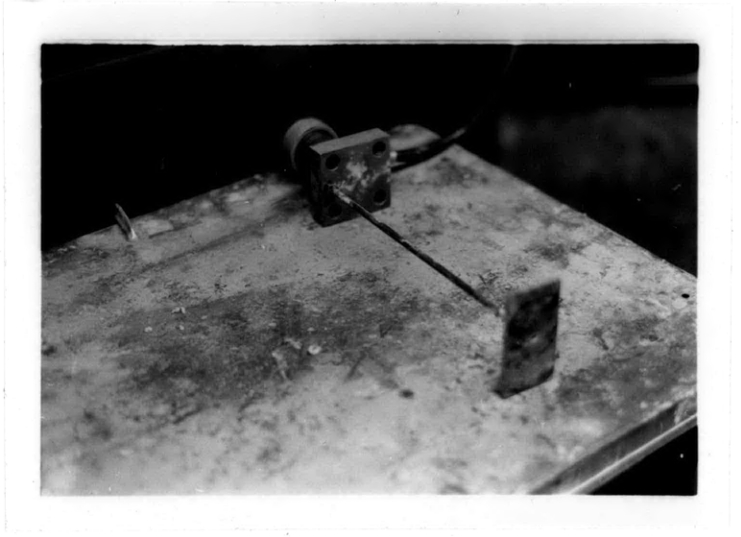

Fig. 12b Vibrating Table and Pneumatic Compacting Tool.

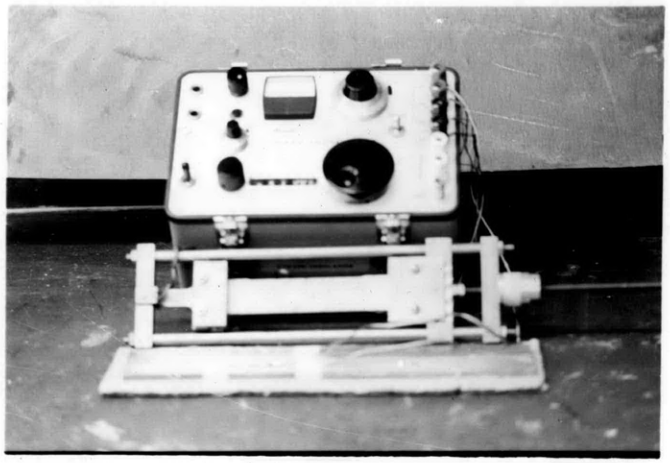

Fig. 12c Straining Device and Strain Indicator.

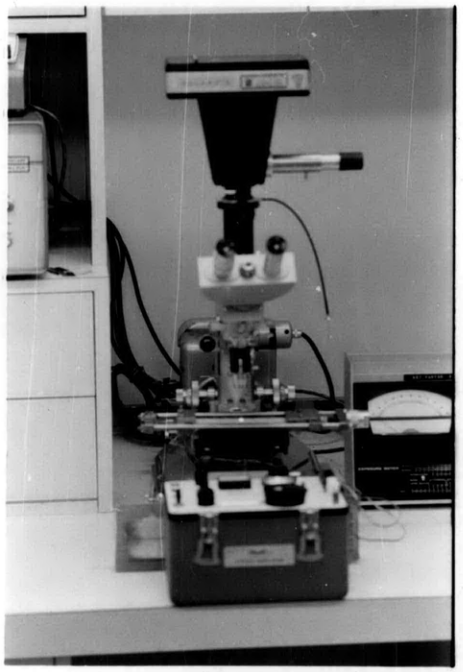

Fig. 12d Straining Device Shown on Microscope Positioning Table.

constructed by using two similar SR-4 compensating gauges and a load cell calibration curve for this system was prepared by hanging known weights from the load cell so supported as to be loaded in tension. Sensitivity was such that load could then be read to the nearest pound force.

3.33 Microscopes

Three microscopes were used for the various stages of specimen study. A variable power 25 X to 100 X (or 50 X to 200 X) stereoscopic microscope by Zeiss was used during the initial straining phase until the first crack appeared because of its superior field of view and great depth of field.

A Reichart Binocular set up for reflected light from the xenon light source was used for detailed study of the crack and for recording significant findings with the Polaroid camera attachment. Used with the reflected light attachment this microscope has lens combinations yielding magnifications from 35X to 550X. Magnifications in excess of 330X yield too little depth of field for use with concrete, however.

The Scanning Electron Microscope by JEOLCO (USA) Inc., was used to a limited extent to study the fracture surface of specimens and post straining sections taken from various locations in tested specimens. It has magnifications from 30X to 30,000X but its principal advantage for this work was its great depth of field at all magnifications. This enabled

the location of cracks not visible with the optical instruments and the taking of pictures of the rough and uneven fracture faces.

3.34 Specimen Sectioning

Sections were cut from specimens after straining by using the precision diamond saw. Three types of sections were taken: fracture face sections, sections parallel to the stress field and sections perpendicular to the stress field (parallel to fracture face). The parallel and perpendicular sections were polished with silicon carbide paper in descending grit size: 140 to 600. Section surfaces were then dyed with red food coloring and allowed to dry for about 10 minutes. The face was then polished again with #600 grit silicon carbide paper and #1 powdered alumina on a polishing table until the surface was a light pink. Any cracks visible with the naked eye remained a deep red. Specimens to be studied with the scanning electron microscope were vacuum impregnated or "shadowed" with gold and mounted with aluminum foil in S.C.M. specimen holders. Silver paint from the foil to the gold plated specimen surface insured a good electrical circuit.

3.40 Testing Procedure

3.41 Specimen Selection

Tests of twenty-seven tensile specimens were recorded;

See Table 1 for detailed description of each specimen. Accidental breakage, excess porosity in samples and lack of time prohibited duplication of tests for each specimen type. Thus, the best specimen of each type was used and the second was saved as a spare.

3.42 Straining Rate and Relaxation

The tendency of the stress in concrete to relax when subjected to a fixed strain made it very difficult to record accurate stress-strain data. Thus elongation was applied in 0.0005 inch increments and the strain indicator deflection meter was zeroed to indicate stress (load cell strain) at that instant. Depending on the time between increments of elongation, the present stress level and the initiation or propagation of a crack, the relaxation of indicated stress varied from 0 to 50 pounds force.

3.43 Recording of Crack Propagation Data

About 150 pictures were taken of the crack initiation/propagation process for the 27 specimens. This is far more than is actually usable in a presentation or discussion of results but the redundancy of pictures served to establish patterns and to teach the observer to look for certain behavior if it had been noted on previous specimens. This technique was an expensive way to record data but proved worthwhile in the long run because the very redundancy of pictures

TABLE 1

Description of Test Specimens

Specimen Number	C/S Ratio	Wire Type	# Layers	Wire Spacing (inches)	Cross Section Area (sq. in.)	Wire Area (sq. in.)	Volume % Steel
1	0.4	SS	1	0.08	0.1095	0.00113	1.03
2	0.4	SS	1	0.10	0.092	0.00102	1.11
3	0.4	SS	1	0.12	0.101	0.0009	0.89
4	0.4	MW	1	0.08	0.131	0.00113	0.86
5	0.4	MW	1	0.10	0.113	0.00102	0.9
6	0.4	MW	1	0.12	0.120	0.00090	0.75
7	0.4	SS	2	0.08	0.141	0.00215	1.42
8	0.4	SS	2	0.10	0.173	0.001924	1.11
9	0.4	SS	2	0.12	0.1785	0.001695	0.95
10	0.4	MW	2	0.08	0.1874	0.0215	1.15
11	0.4	MW	2	0.10	0.140	0.00192	1.37
12	0.4	MW	2	0.12	0.163	0.001695	1.04
13	0.4	GALV	2	0.08	0.168	0.00215	1.28
14	0.4	GALV	2	0.10	0.193	0.00262	1.35
15	0.7	SS	2	0.10	0.102	0.00215	2.1
16	0.7	SS	2	0.10	0.1015	0.001924	1.9
17	0.7	MW	2	0.08	0.225	0.00215	0.96
18	0.7	MW	2	0.10	0.168	0.00192	1.28
19	0.7	MW	2	0.10	0.1825	0.00192	1.05
20	0.7	GALV	2	0.08	0.167	0.00293	1.75
21	0.7	GALV	2	0.10	0.153	0.00262	1.72
22	0.7	SS	Chopped	0.11	0.237	-	2
23	0.4	SS	Chopped	0.11	0.198	-	2
24	0.4	MW	Chopped	0.11	0.218	-	2
25	0.7	MW	Chopped	0.11	0.210	-	2
26	0.4	GALV	Chopped	0.13	0.230	-	2.7
27	0.7	GALV	Chopped	0.13	0.204	-	2.7

served as additional incentive to search for new things to photograph.

3.44 Wire and Pullout Tests

The Instron Universal Testing Machine was used to test the pullout specimens for wire bond strength and to determine the yield strength and ultimate tensile strengths of the three wire types. The low range load cell was installed and the crosshead speed set at 0.05 inches per minute. The recorder was set at full scale deflection of 50 pounds and the paper advance speed at 1 inch per minute. For the wire strength tests, the initial specimen length between grips was adjusted to 1 inch so that Youngs Modulus could be calculated directly from elongation vs. stress.

IV. RESULTS

4.1 Tensile Tests

Description and data for all tensile tests are contained in Appendix A and the stress-strain diagrams of Figures 13 through 18 summarize the tensile test results for representative wire types and spacings in both lean and rich mixes of mortar.

4.2 Photographs

Figures 19 through 27 illustrate the results of visual observation of the tensile tests. Approximately 150 additional photographs were taken of the 27 test specimens and were used in assembling these representative groups. The additional photographs are mounted and bound under separate cover (38) which is available for reference.

4.3 Wire Pullout Tests

Summarized in Table 2.

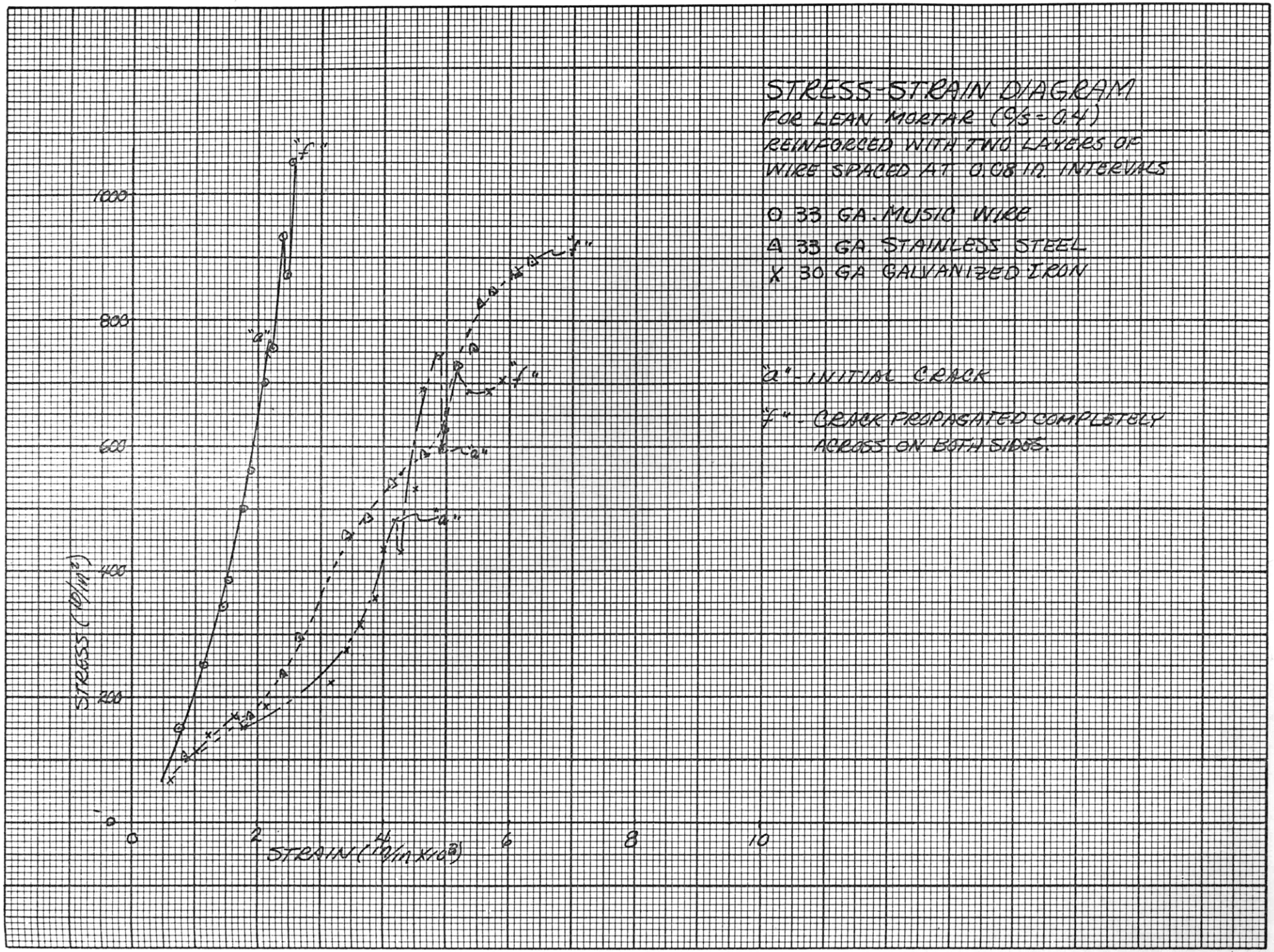
STRESS-STRAIN DIAGRAM
FOR LEAN MORTAR (C/S = 0.4)
REINFORCED WITH TWO LAYERS OF
WIRE SPACED AT 0.08 IN. INTERVALS
O 33 GA. MUSIC WIRE
Δ 33 GA. STAINLESS STEEL
X 30 GA GALVANIZED IRON
"a" - INITIAL CRACK
"f" - CRACK PROPAGATED COMPLETELY ACROSS ON BOTH SIDES.
STRESS (lb/in²)
STRAIN (in/in x 10³)
1000
800
600
400
200
0
2
4
6
8
10
"f"
"a"

Figure 13

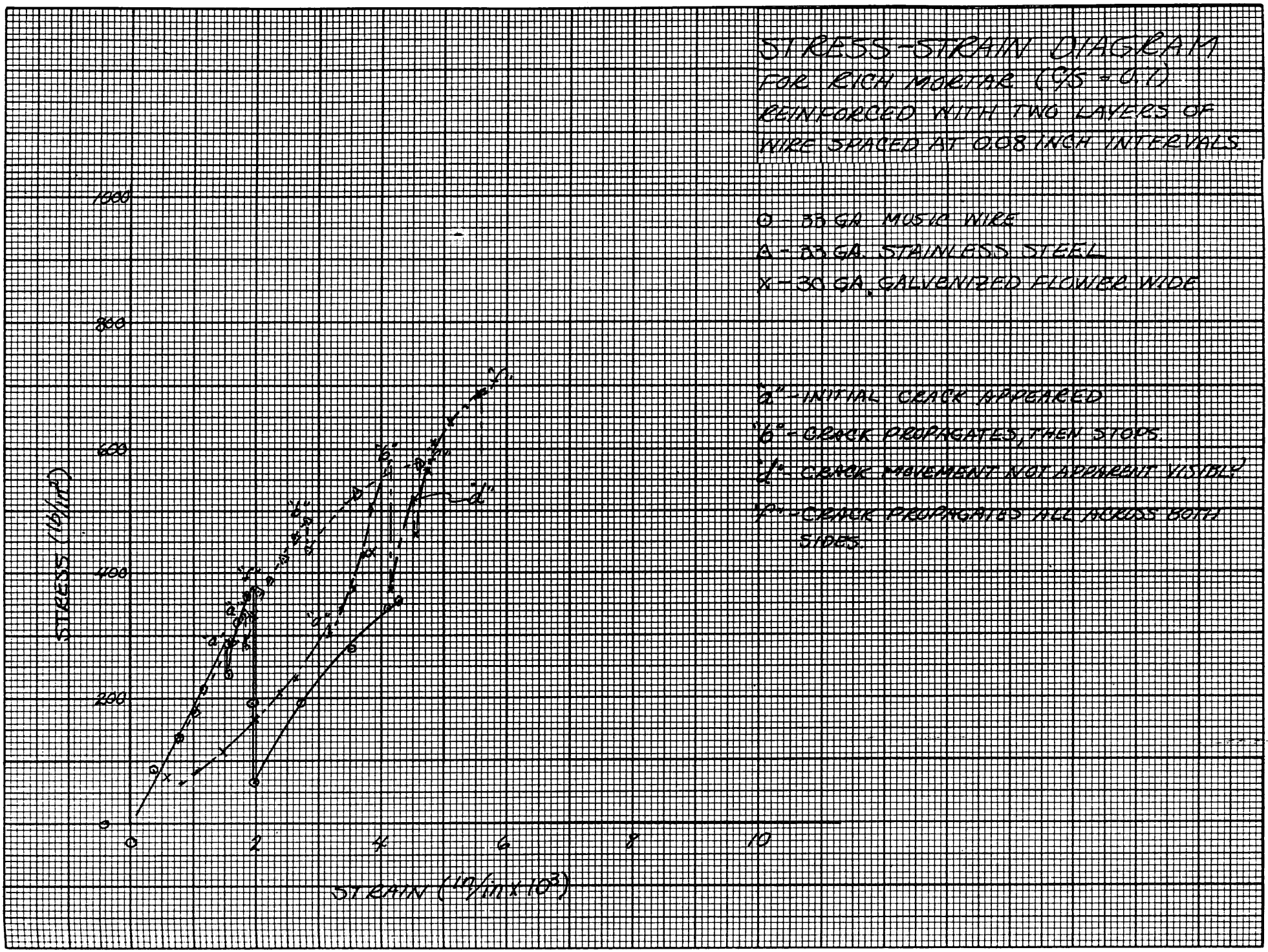
STRESS-STRAIN DIAGRAM
FOR RICH MORTAR (C/S = 0.7)
REINFORCED WITH TWO LAYERS OF
WIRE SPACED AT 0.08 INCH INTERVALS.
○ - 35 GA. MUSIC WIRE
△ - 23 GA. STAINLESS STEEL
× - 30 GA. GALVANIZED FLOWER WIRE
"a" - INITIAL CRACK APPEARED
"b" - CRACK PROPAGATES, THEN STOPS.
"c" - CRACK MOVEMENT NOT APPARENT VISIBLY
"f" - CRACK PROPAGATED ALL ACROSS BOTH SIDES.
STRESS (lb/in²)
STRAIN (in/in × 10³)
0
200
400
600
800
1000
2
4
6
8
10

Figure 14

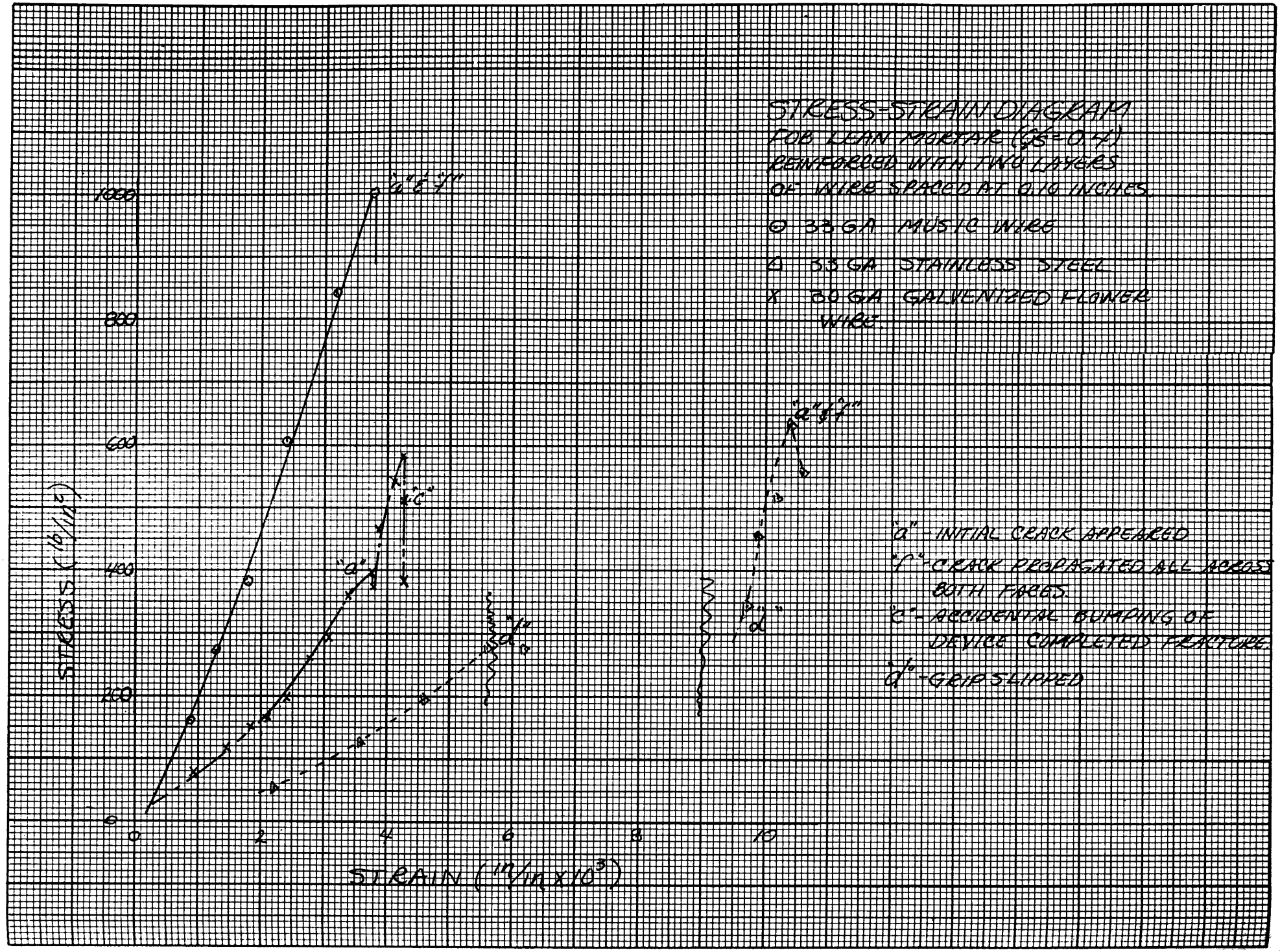
STRESS-STRAIN DIAGRAM
FOR LEAN MORTAR (C:S=0.7)
REINFORCED WITH TWO LAYERS
OF WIRE SPACED AT 0.10 INCHES.
○ 33 GA MUSIC WIRE
□ 33 GA STAINLESS STEEL
X 30 GA GALVENIZED FLOWER WIRE.
"a" - INITIAL CRACK APPEARED
"c" - CRACK PROPAGATED ALL ACROSS BOTH FACES.
"c" - SECONDARY BUMPING OF DEVICE COMPLETED FRACTURE.
"d" - GRIP SLIPPED
STRESS (lb/in²)
STRAIN (in/in x 10³)
1000
800
600
400
200
0
0
2
4
6
8
10

Figure 15

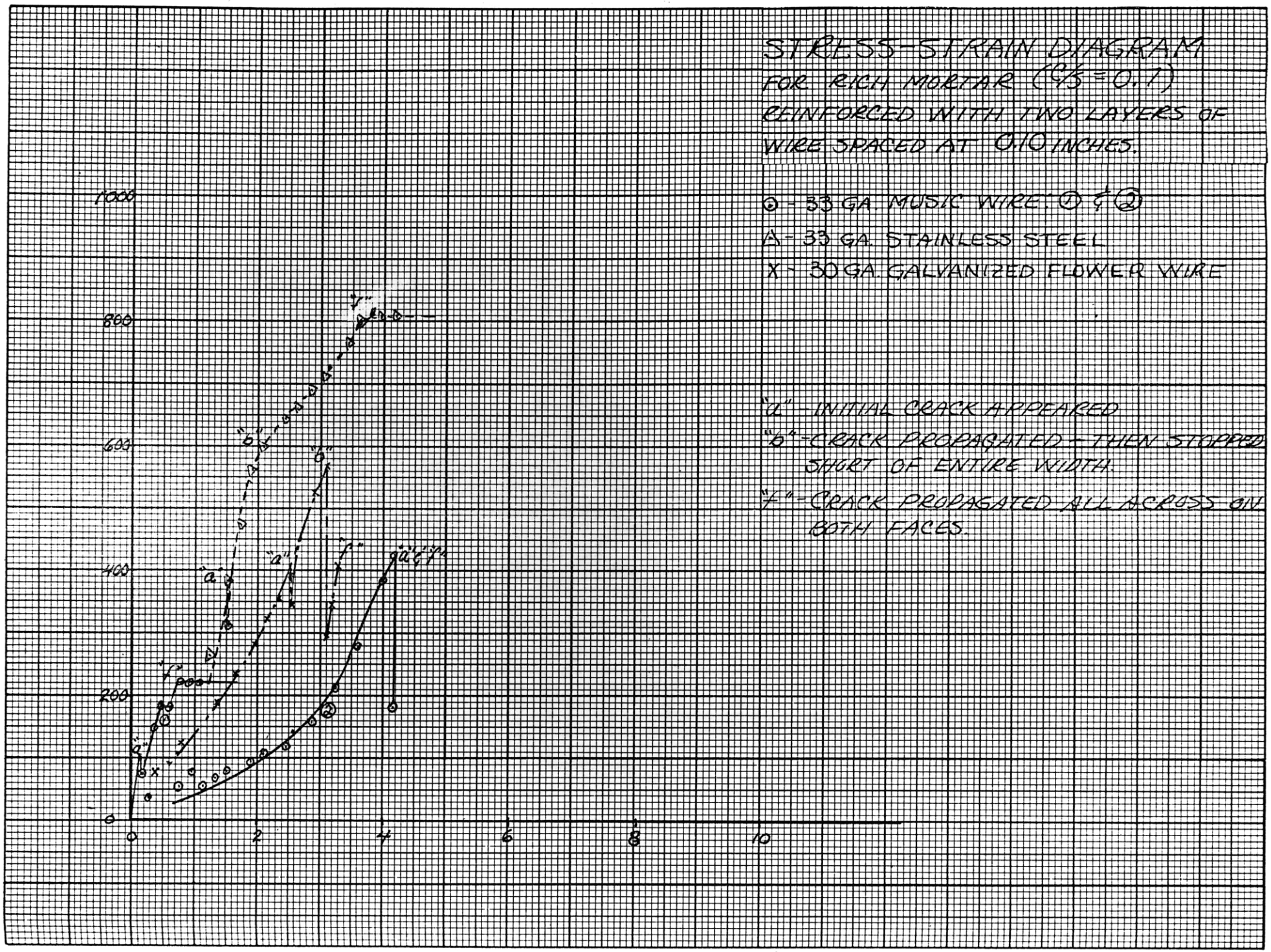
STRESS-STRAIN DIAGRAM
FOR RICH MORTAR (C/S = 0.1)
REINFORCED WITH TWO LAYERS OF
WIRE SPACED AT 0.10 INCHES.
⊙ - 33 GA. MUSIC WIRE. ① & ②
△ - 33 GA. STAINLESS STEEL
X - 30 GA. GALVANIZED FLOWER WIRE
"a" INITIAL CRACK APPEARED
"b" - CRACK PROPAGATED - THEN STOPPED
SHORT OF ENTIRE WIDTH.
"f" - CRACK PROPAGATED ALL ACROSS ON
BOTH FACES.
1000
800
600
400
200
0
2
4
6
8
10

Figure 16

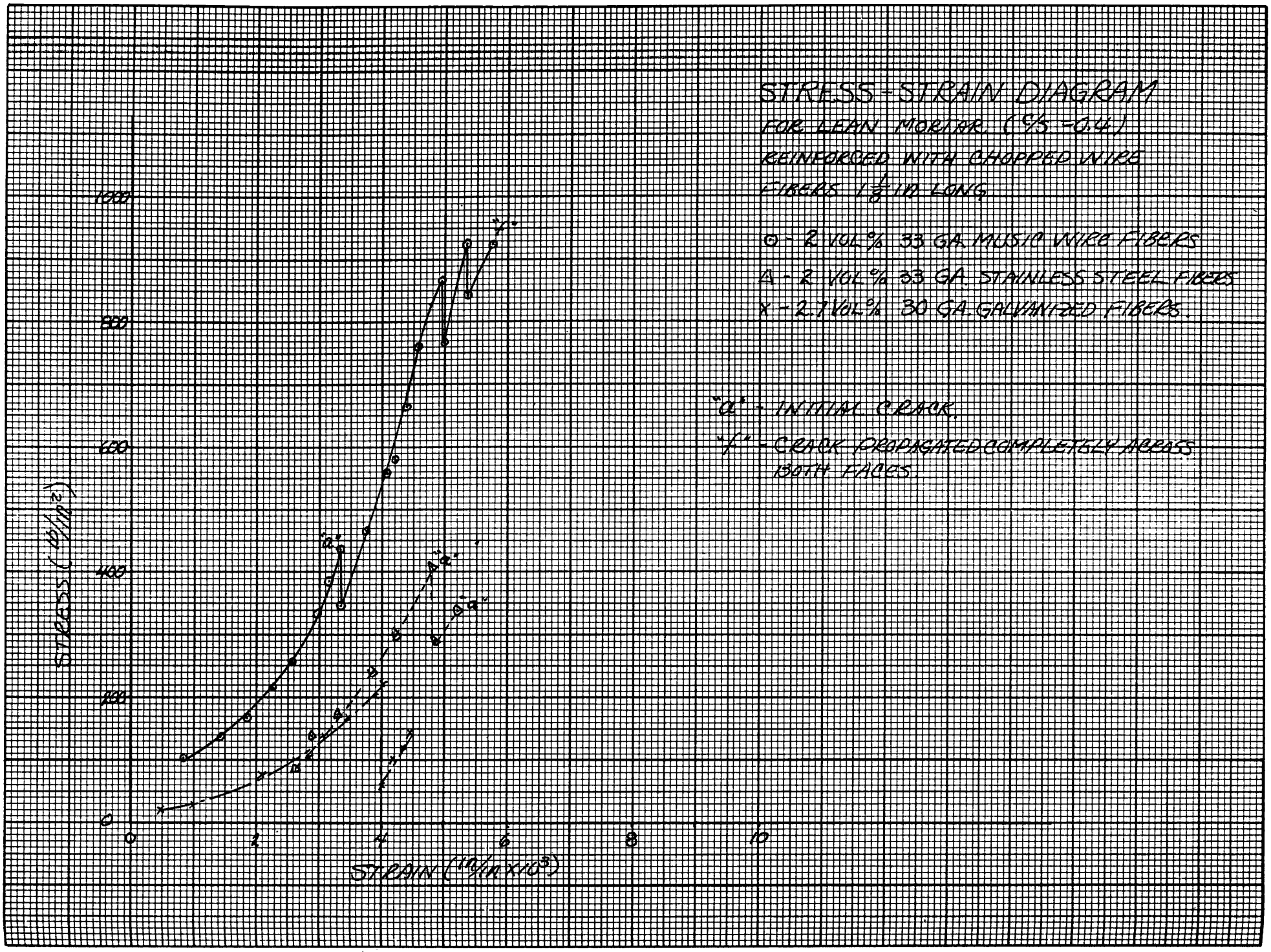
STRESS - STRAIN DIAGRAM
FOR LEAN MORTAR (C/S = 0.4)
REINFORCED WITH CHOPPED WIRE
FIBERS 1½" LONG.
○ - 2 VOL % 33 GA. MUSIC WIRE FIBERS
Δ - 2 VOL % 33 GA. STAINLESS STEEL FIBERS
× - 2.1 VOL % 30 GA. GALVANIZED FIBERS.
"a" - INITIAL CRACK.
"f" - CRACK PROPAGATED COMPLETELY ACROSS BOTH FACES.
STRESS (lbs/in²)
STRAIN (in/in × 10⁻³)
0
200
400
600
800
1000
2
4
6
8
10

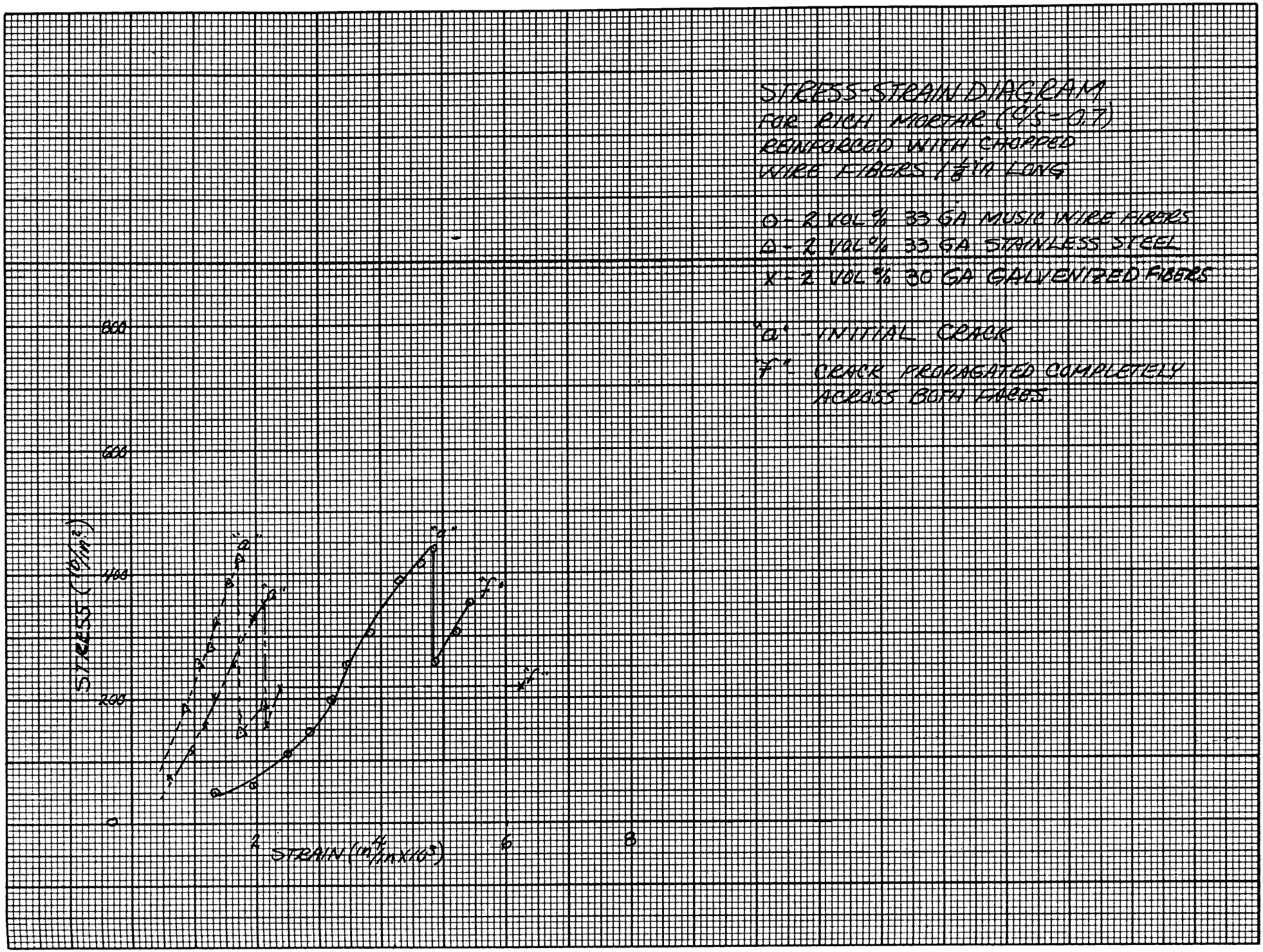
STRESS-STRAIN DIAGRAM
FOR RICH MORTAR (V/S = 0.7)
REINFORCED WITH CHOPPED
WIRE FIBERS 1" IN LONG
O - 2 VOL % 33 GA MUSIC WIRE FIBERS
Δ - 2 VOL % 33 GA STAINLESS STEEL
X - 2 VOL % 30 GA GALVENIZED FIBERS
'a' INITIAL CRACK
'F' CRACK PROPAGATED COMPLETELY ACROSS BOTH FACES.
STRESS (lb/in²)
800
600
400
200
0
2
6
8
STRAIN (in/in x 10³)

Figure 18

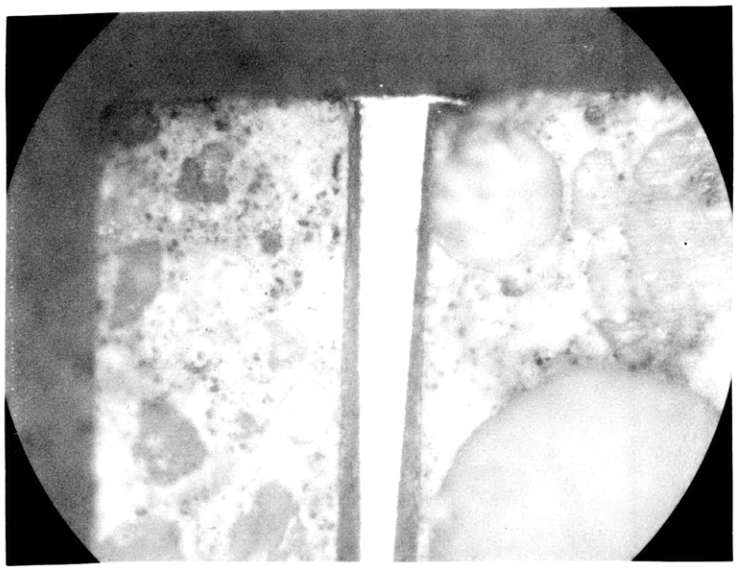

Fig. 19a (Specimen 5) Note wire layer is near surface at right. This sample cracked all across on one side with thick cover when it was only about 45% across on thin cover. (35X)

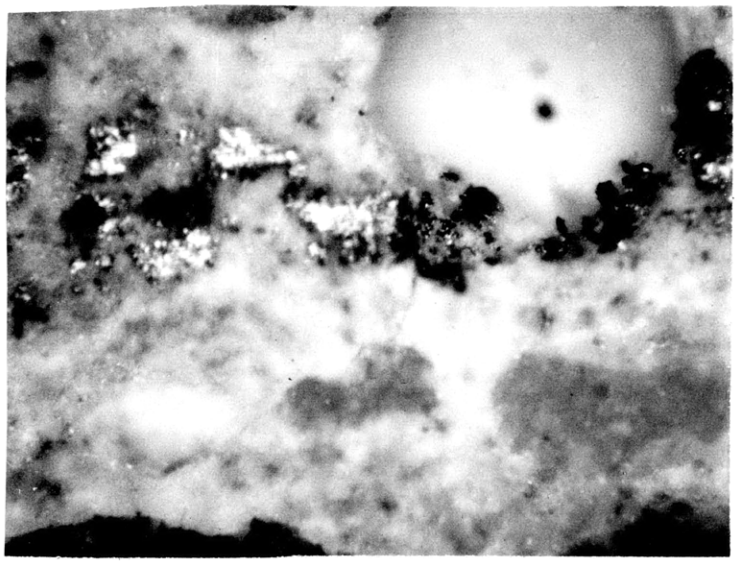

Fig. 19b (Specimen 21) Crack arrested here at black pencil line which marks location of wire. (110X)

Fig. 19c (Specimen 24) Crack arrested here by partly uncovered wire. (220X)

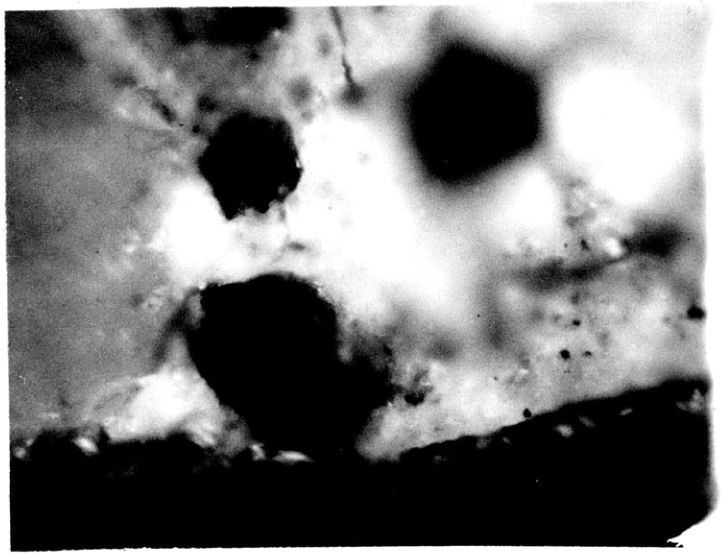

Fig. 19d (Specimen 24) Sample stressed enough to noticeably open crack but it still did not propagate past wire. (220X)

Figure 19 - Arrest by Wire

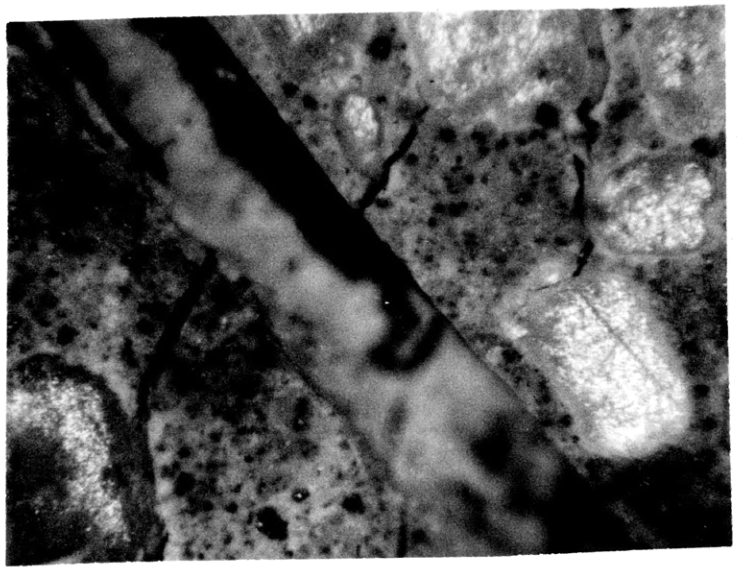

Fig. 20a (Specimen 27) Cracks jump wire in direction perpendicular to wire if bond is good. (55X)

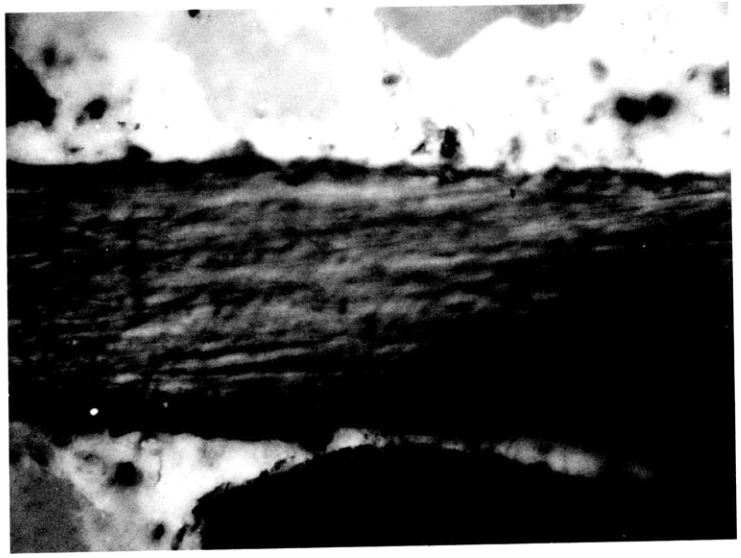

Fig. 20b (Specimen 20) Less marked tendency to jump wire in perpendicular direction if bond is poor. (110X)

Figure 20 - Cracks Cross Wires in Perpendicular Direction.

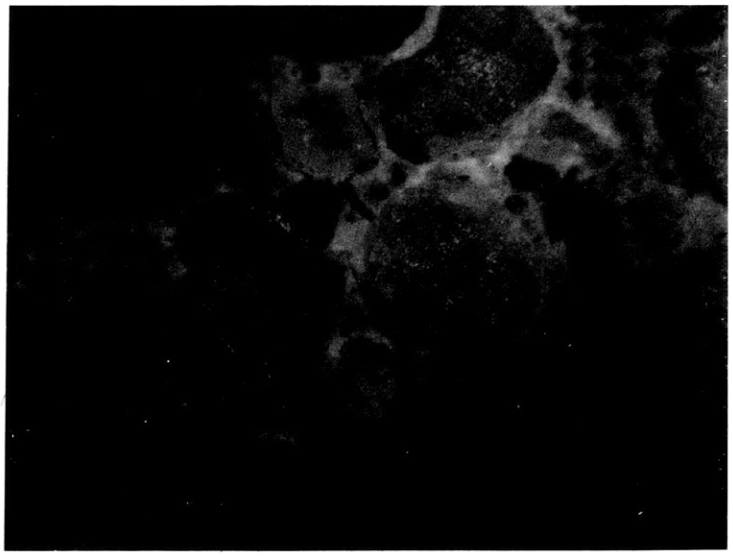

Fig. 21a (Specimen 14) Preferred crack propagation route is weak interfaces. (55X)

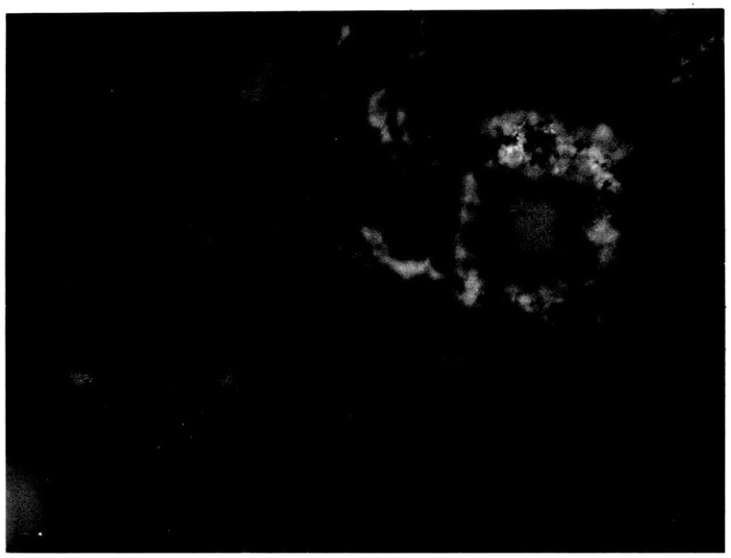

Fig. 21b (Specimen 2) Crack surrounds aggregate, enters void and continues to propagate. (110X)

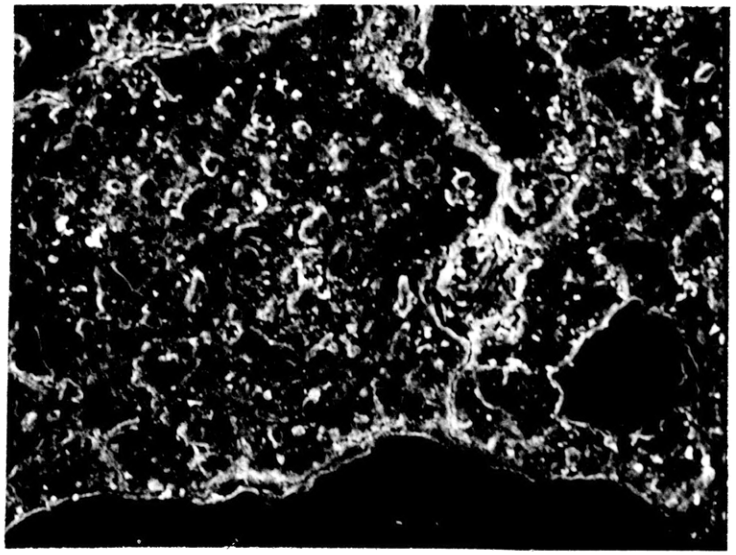

Fig. 21c (Specimen 12) Crack travels across matrix to weak bond interface in two directions - general failure beginning. (SEM at 250X)

Figure 21 - Preferred Routes of Travel for Cracks

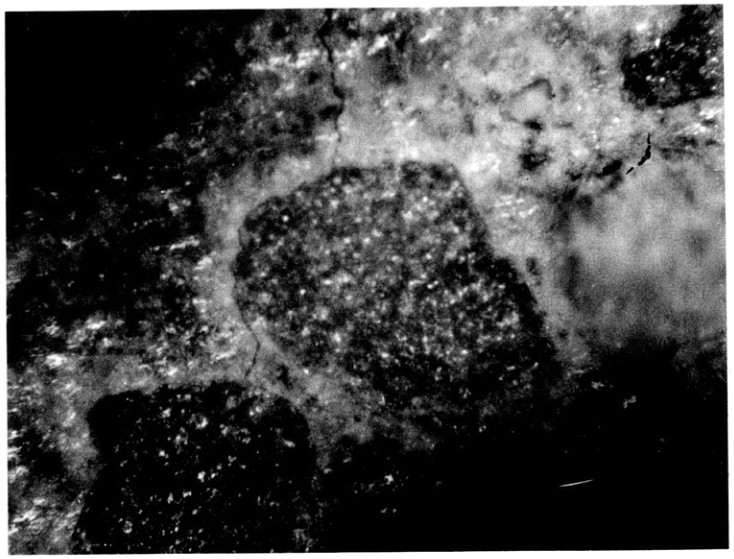

Fig. 21d (Specimen 18) Preferred crack propagation path is straight through matrix except to detour around solid aggregate through the weaker interface. (110X)

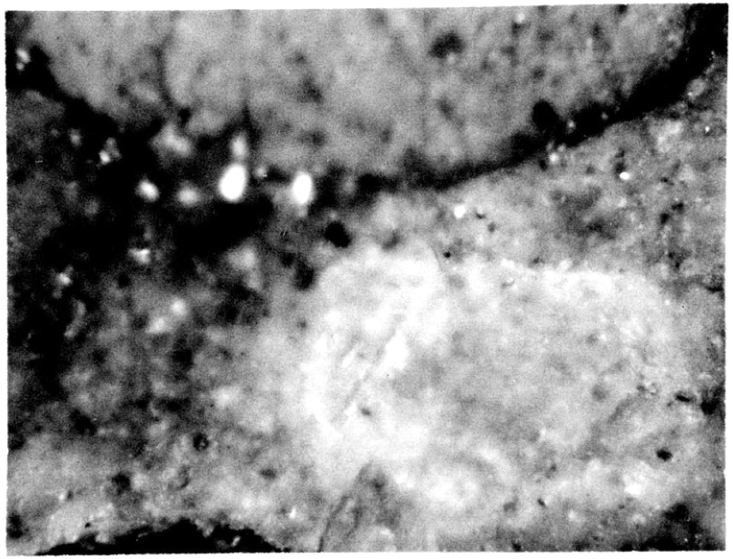

Fig. 21e (Specimen 25) If aggregate is broken, there is no need to detour. (220X)

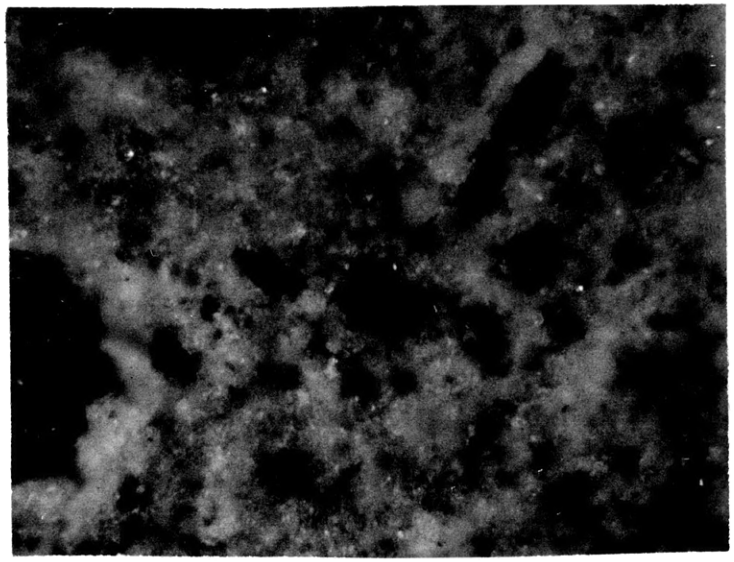

Fig. 21f (Specimen 23) Cracks in chopped wire specimen meander more aimlessly than parallel wire specimens, believe this is due to preference of crack to propagate around and past wire in perpendicular direction. (220X)

Figure 21 - (Cont'd)

Fig. 22a (Specimen 24) Chopped wire specimens have more branching than continuous specimens. Each of these two branches goes all across front and back and each has two sub-branches. (110X)

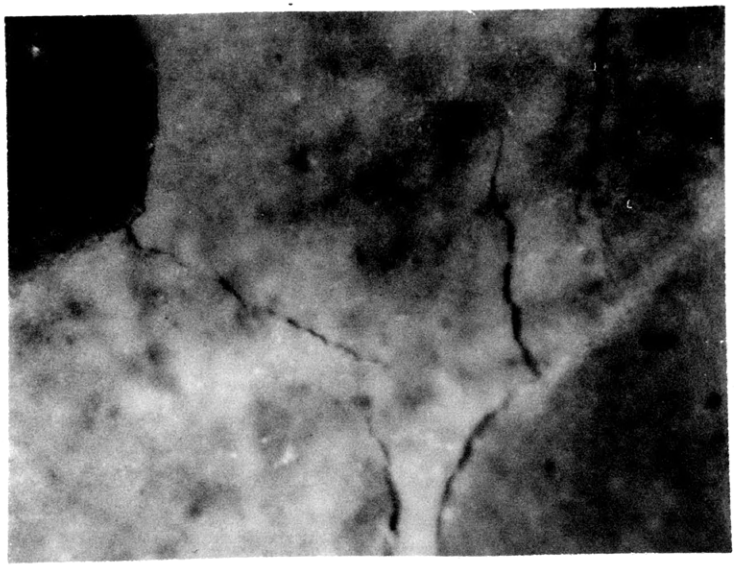

Fig. 22b (Specimen 16) This parallel wire specimen was characterized by porosity and shrinkage cracks. Resulted in some branching. (110X)

Figure 22 - Branching of Cracks

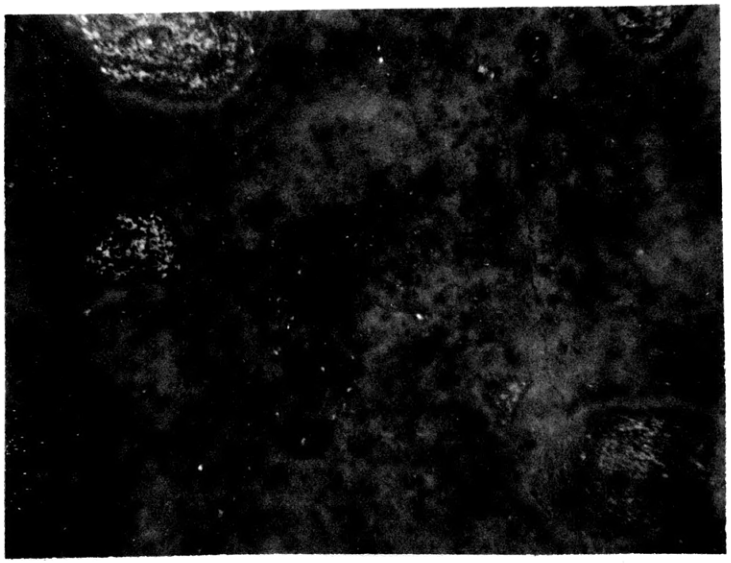

Fig. 23a (Specimen 25) Two parallel cracks exchange role as principal failure path near center of specimen. (55X)

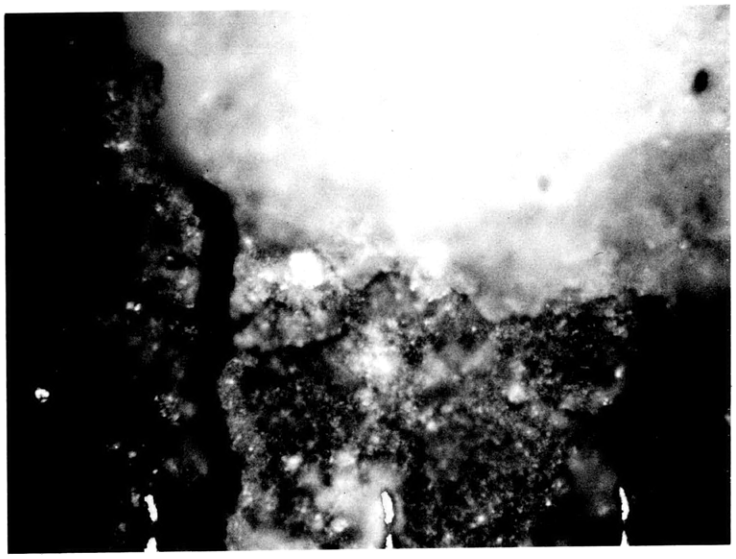

Fig. 23b (Specimen 11) Typical pattern for joining of major crack pair (220X)

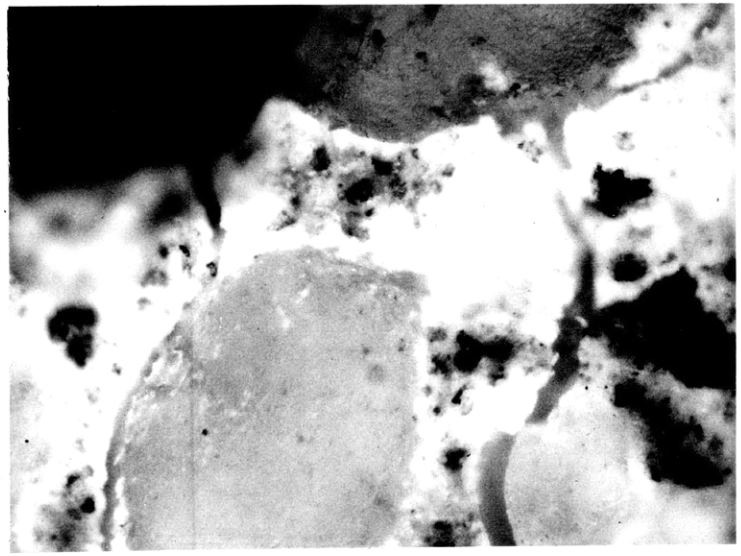

Fig. 23c (Specimen 22) Crack pair start from different locations in notch with brittle break - opening wide (110X)

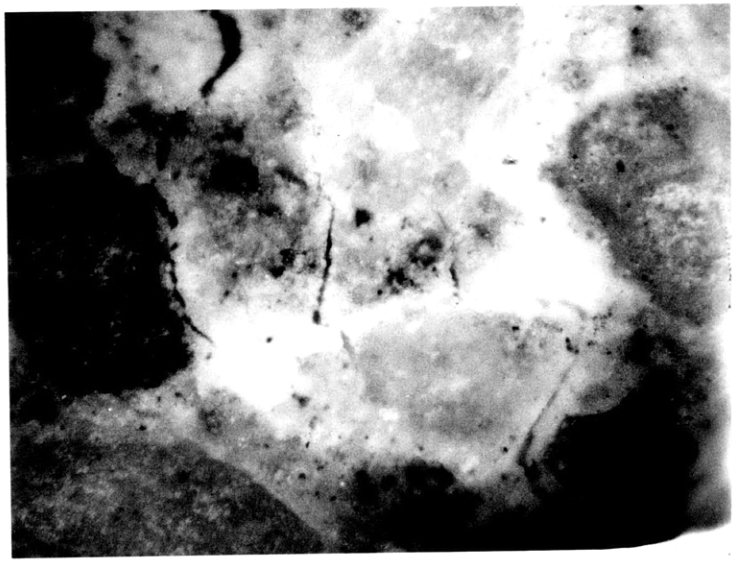

Fig.23d (Specimen 5) Three crack parallel array in exchanging role as major failure path. (110X)

Figure 23 - Pairing

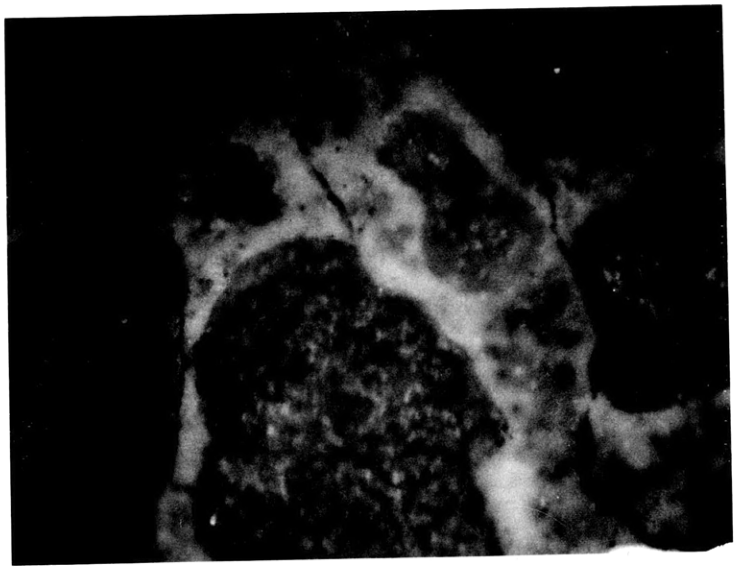

Fig. 23e (Specimen 1) Major disruption after straining frame was bumped. (110X)

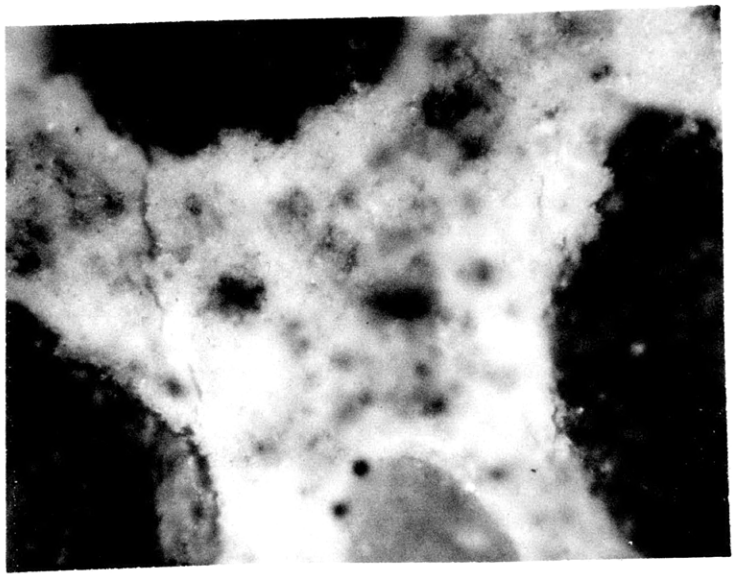

Fig. 23a (Specimen 4) Pairing takes place here near the stress raising notch. (220X)

Fig. 23g (Specimen 12) Pairing seems to be more prevalent in music wire reinforced specimens. (330X)

Figure 23 (Cont'd) - Pairing

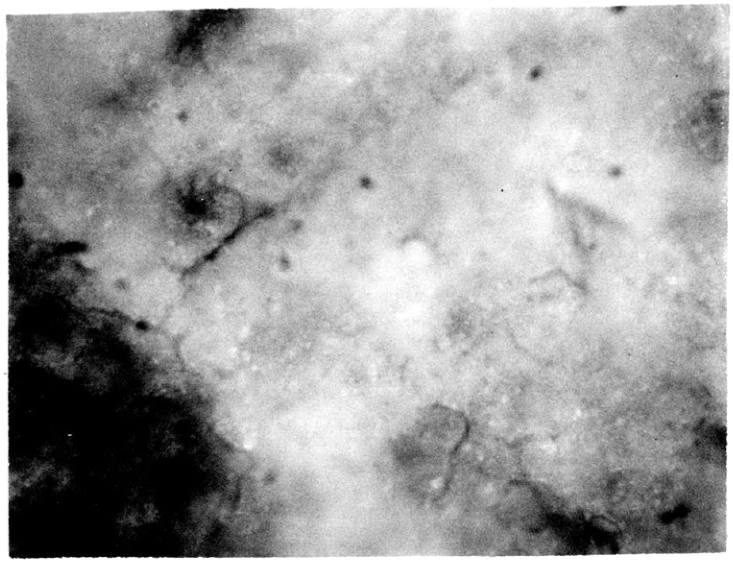

Fig. 24a (Specimen 16) Shrinkage cracking on this face is initiation site for second of main crack pair. (440X)

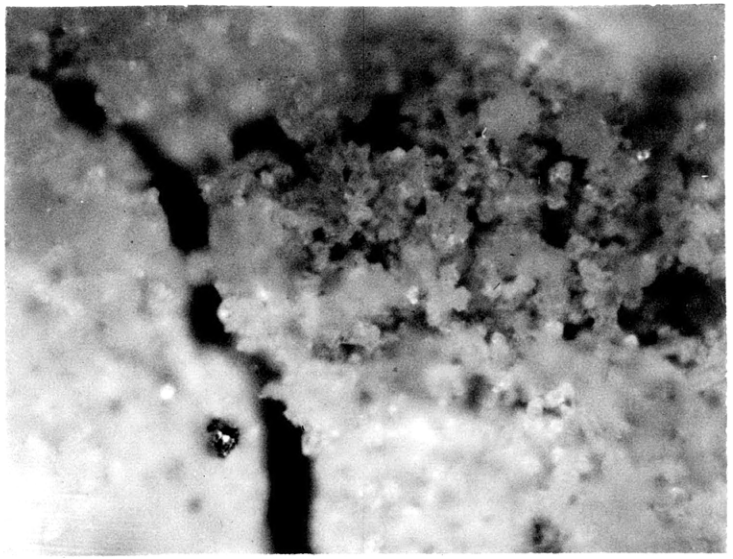

Fig. 24b (Specimen 16) Microporosity on opposite face from shrinkage cracking. (220X)

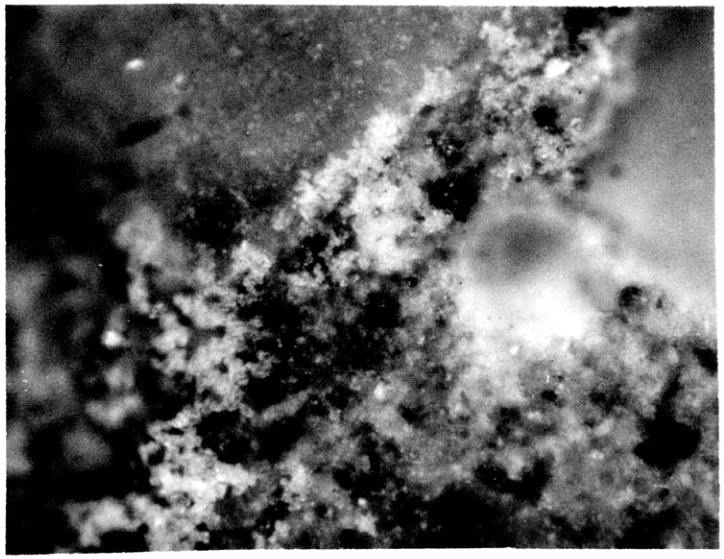

Fig. 24c (Specimen 15) Care must be exercised to avoid segregation and microporosity in rich mixes. (220X)

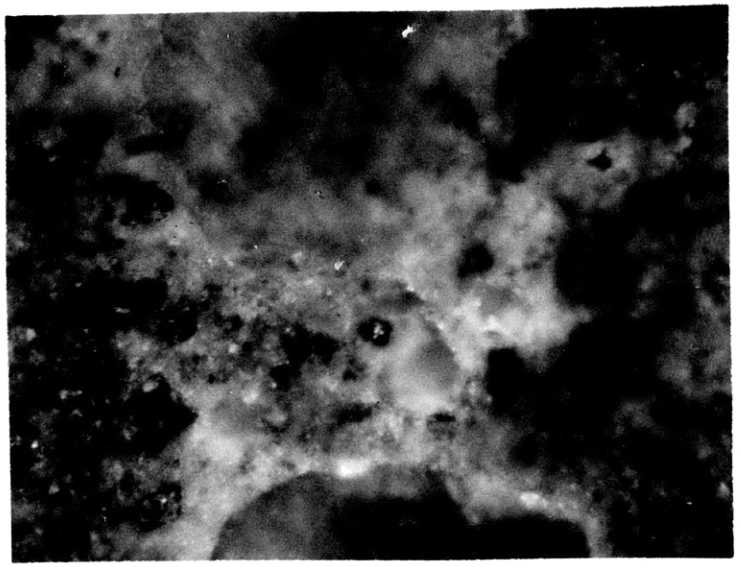

Fig. 24d (Specimen 23) Segregation and microporosity again in rich mix. (220X)

Figure 24 - Microporosity and Shrinkage Cracking

Fig. 25a (Specimen 13) General failure of paste - aggregate interface in this region. (SEM @ 250X)

Fig. 25b (Specimen 5) Poor paste aggregate interface bond causes crack to surround this particle as specimen fractured all across. (110X)

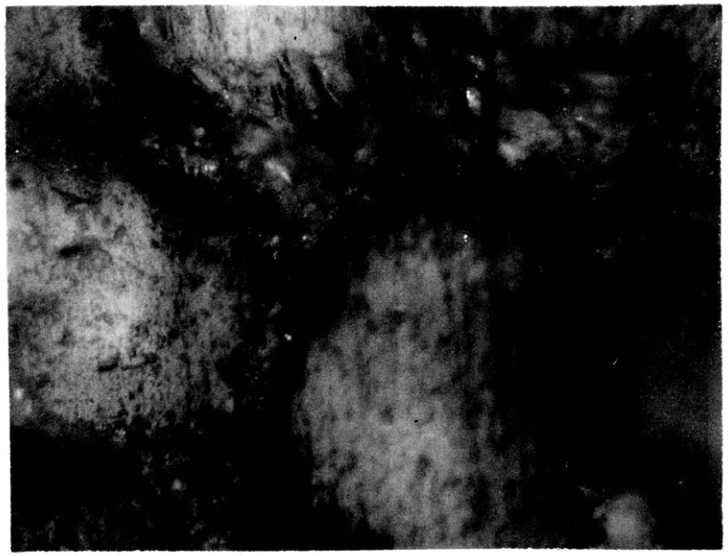

Fig. 25c (Specimen 10) Extensive microcracking and segregation in parallel section. (220X)

Figure 25 - Interface Cracking

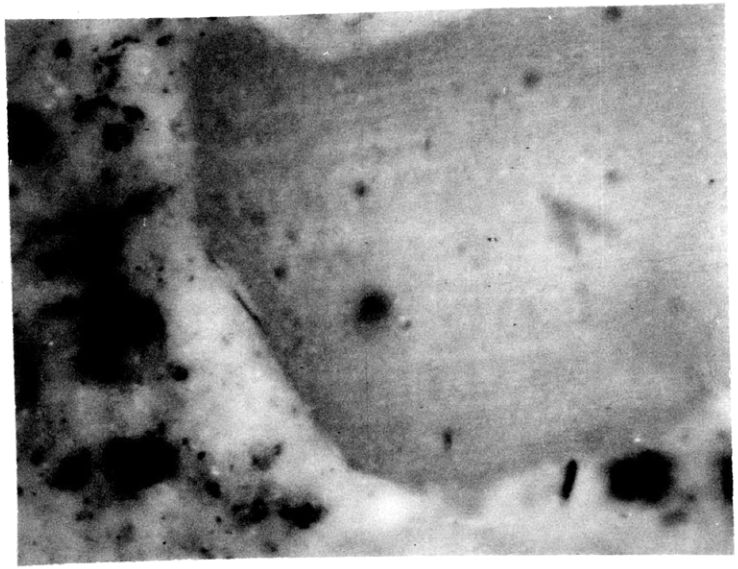

Fig. 25d (Specimen 5) Parallel section showing microcrack at interface. (220X)

Fig. 25e (Specimen 2) Microcracks and segregation at interface in this post straining parallel section. (220X)

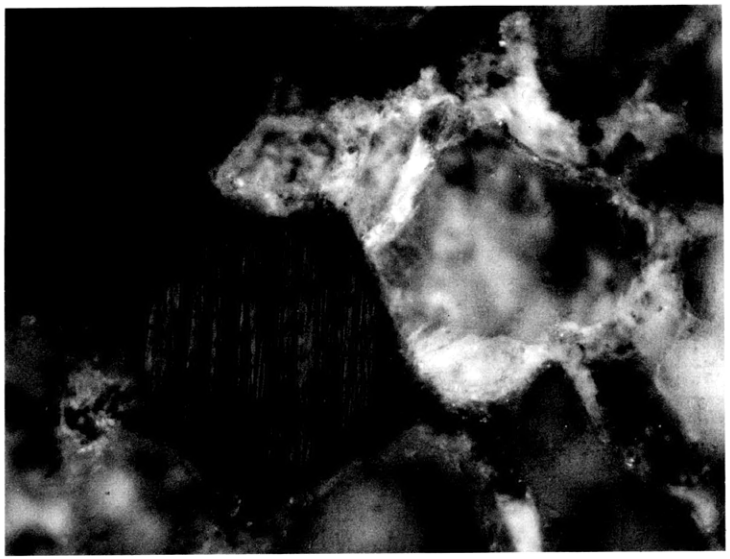

Fig. 25f (Specimen 10) Interface crack in perpendicular cross section after straining. (110X)

Figure 25 (Cont'd) - Interface Cracking

Fig. 26a (Specimen 13) Fracture surface separated from other half with pliers. Note cementitious material still bonded to the wire surface. (SEM @ 250X)

Fig. 26b (Specimen 23) Note excellent bonding here where surface is polished away from wire. (220X)

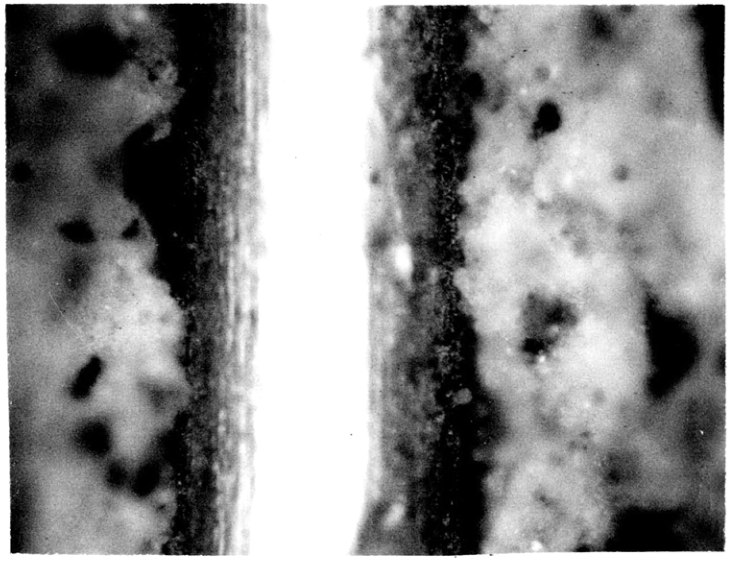

Fig. 26c (Specimen 17) Less efficient bond here may be due to disruption caused by diamond saw vibrating the stiff wire. (220X)

Figure 26. Wire Bonding

Fig. 26d (Specimen 27) Outstanding bond here shown just as polishing has bared some spots of wire. (220X)

Fig. 26e (Specimen 22) Note crack propagating in paste-wire interface with poor bond. (220X)

Figure 26 (Cont'd) - Wire Bonding

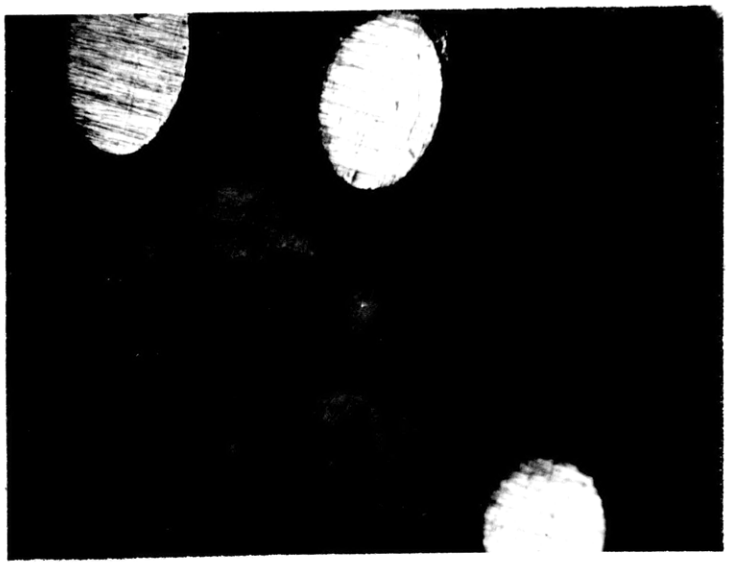

Fig. 27a (Specimen 24) Chopped wires appear to bunch up. Wires also appear to attract air bubbles. (55X).

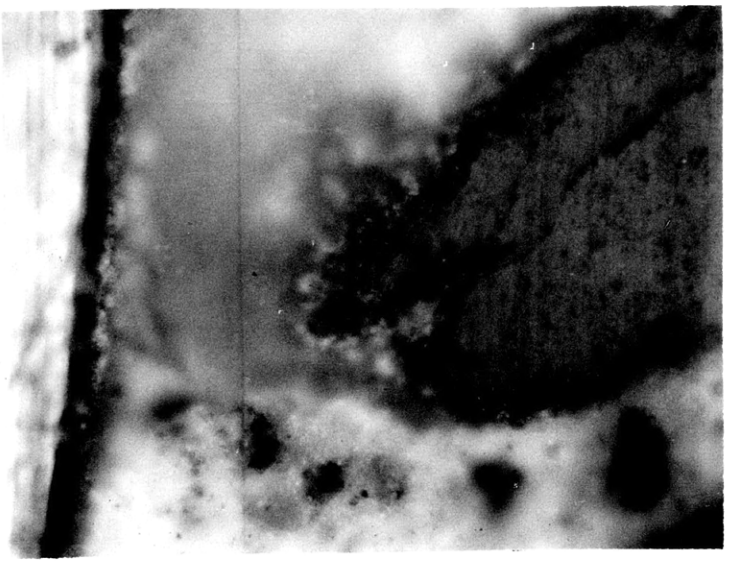

Fig. 27b (Specimen 2) Air Pocket and segregation near wire here. (220X)

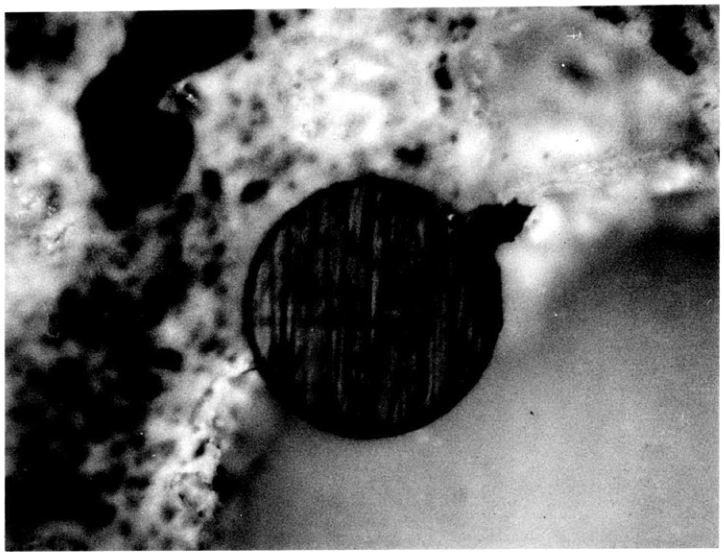

Fig. 27c (Specimen 10) Small microcrack near edge of void which is adjacent to wire. (110X)

Fig. 27d (Specimen 23) Secondary crack started from wire - void pocket near center of specimen - traveled about 0.1" and stopped. (220X)

Figure 27 - Wires Attract Air Bubbles

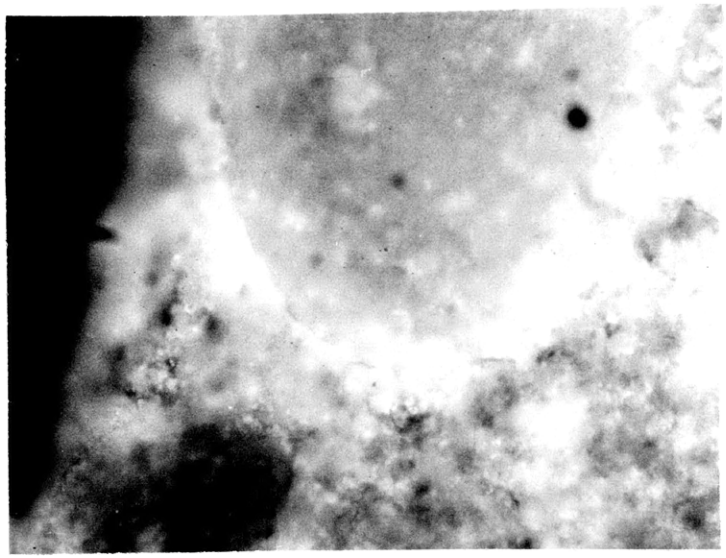

Fig. 28a (Specimen 21) This crack started from side of notch - believed due to notch cutting through wire located here. (220X)

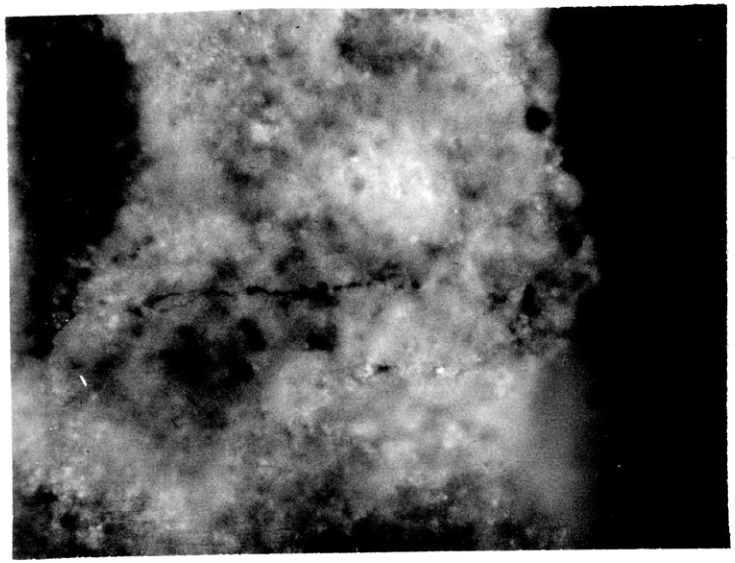

Fig. 28b (Specimen 21) Crack in corresponding position on opposite side of notch. Neither crack appeared until heavy load was applied. (220X)

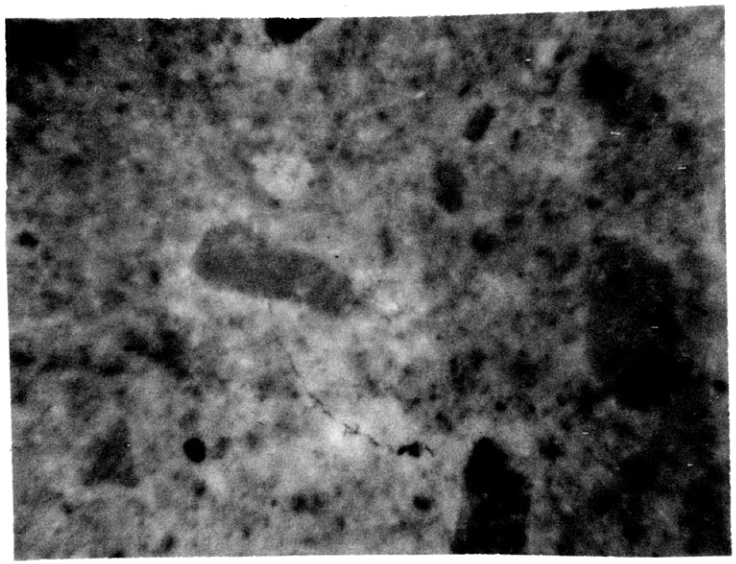

Fig. 28c (Specimen 21) At about 10% across width, 45° crack changes to 90° crack - roughly where crack met the next wire. (220X)

Figure 28 - Cracks Parallel to Stress Field

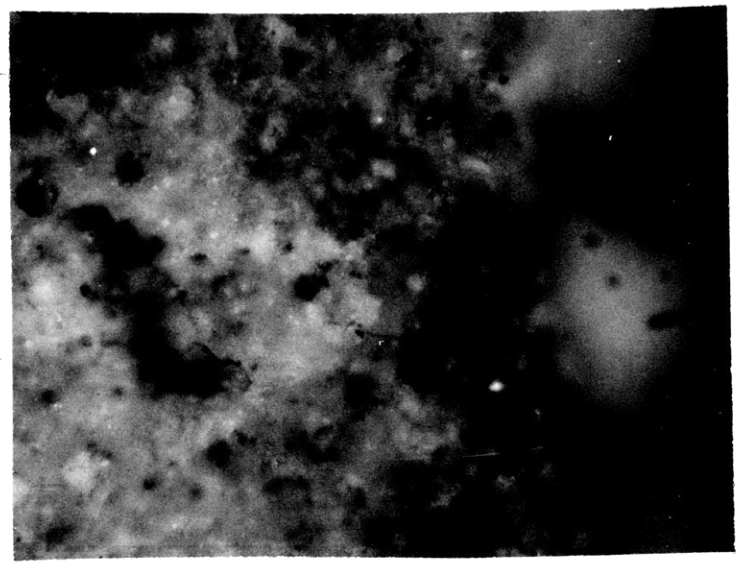

Fig. 28d (Specimen 20) Crack originating in large void and propagating parallel to stress field and wires. (220X)

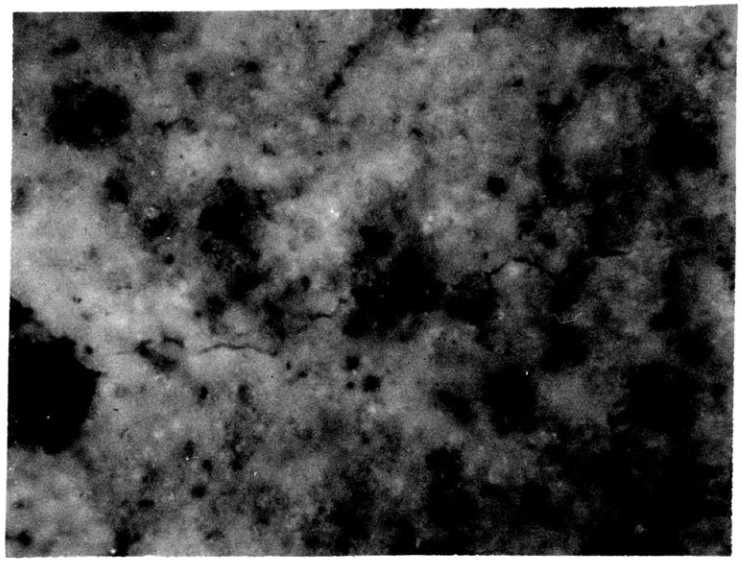

Fig. 28 e (Specimen 20) Another longitudinal crack on opposite side of same void. A wire very near the surface is in line with this crack. (220X)

Figure 28 (Cont'd) - Cracks Parallel to Stress Field

Fig. 29a (Specimen 13) Fracture surface view showing irregularity of crack in three dimensional space. (SEM at 60X)

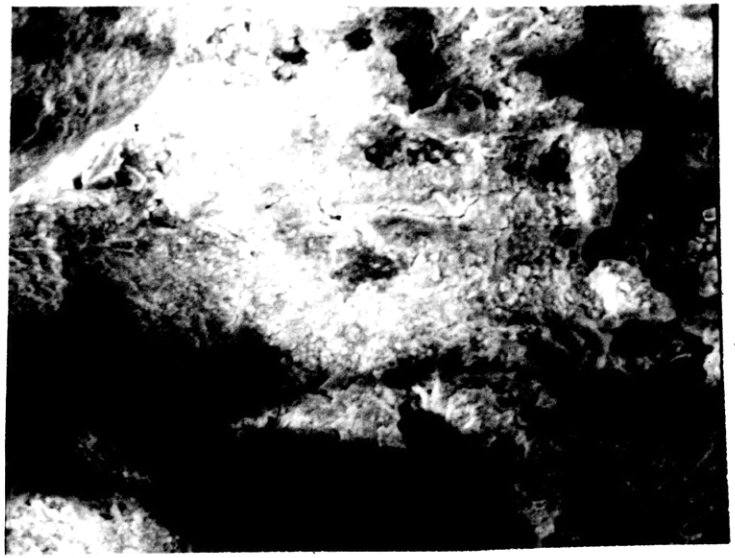

Fig. 29b (Specimen 13) Crack in fracture surface extends in direction parallel to wires and stress field. Indicates general failure in this region.(SEM at 250X)

Fig. 29c (Specimen 13) Same fracture surface crack at 600X.

Figure 29 - Fracture Surface

TABLE 2

Results of Wire Pullout Tests

Specimen Behavior	Test Number	Wire Stress (psi) at Indicated Behavior					
		Lean Mortar			Rich Mortar		
		SS	Galv	MW	SS	Galv	MW
Yield	1	57,500	39,000	230,000	57,500	39,000	-
	2	57,500	39,000	230,000	57,500	39,000	-
	Avg.	57,500	39,000	230,000	57,500	39,000	-
Wire Rupture	1	101,000	46,000	-	100,000	46,000	-
	2	103,000	* -	-	-	48,000	217,000
	Avg.	102,000	46,000	-	100,000	47,050	217,000
Initial Wire Pullout	1	-	-	258,000	-	-	226,000
	2	-	-	277,000	86,500	-	-
	Avg.	-	-	267,500	86,500	-	226,000
Average Friction of Sliding Wire	1	-	-	159,000	-	-	88,500
	2	-	-	71,000	73,500	-	-
	Avg.	-	-	115,000	73,500	-	88,500

- Specimen did not show indicated behavior.

* Wire was rusted nearly through at junction with mortar and snapped off prior to testing.

V. DISCUSSION OF RESULTS

5.1 Stress Strain Diagrams

Figures 13 through 18 verify that cracking did not occur in regions remote from the notch except in isolated instances already noted in section V. The visual observation of the initiation or unstable propagation of a crack correlates in nearly every case with the sudden dips in the stress-strain diagram. Gradual relaxation due to the time dependent behavior of concrete is difficult to distinguish from the nonlinear character of the modulus of elasticity. The accuracy of the stress-strain data is prejudiced to an uncertain degree for this reason. The time between straining increments varied greatly due to the variation of time needed to study crack propagation behavior in different regions. At the time these data were taken, the importance of this gradual relaxation was greatly overestimated, however, due to the sensitivity of the strain indicator. It was felt that the stress-strain information would be good only for order of magnitude comparisons so many tests were stopped when visual observations were complete. This is unfortunate because the accuracy of the stress-strain data has proven reasonably good and more could be gained from analysis if all tests had been run to completion of the crack propagation.

5.2 Analysis of Stress-Strain Results

The shape of the stress-strain diagram for galvanized wire in Figure 13 suggests that wire pullout may have occured so an attempt was made to correlate the wire pullout test results with the tensile tests. Table 3 and 4 show the results of this analysis.

It is a reasonable assumption that at the time stable crack propagation is very nearly 100% across the specimen the wires are carrying essentially all of the load. As a comparison, this same assumption was then applied to the condition at incipient crack initiation.

For the chopped wire specimens, the effective number of wires at a unit cross sectional area was computed with the formula $n_w = \frac{1}{S^2}$ taken from Romualdi and Mandel (34). S was already computed with $S = 13.8\ d\sqrt{\frac{1}{p}}$ and tabulated in Table 1. The scatter diagram in Figure 30 indicates that for lean mortar specimens, the formation of a crack completely across the specimen may well be dependent upon yielding of the wire reinforcement. Note, however, that the high strength, cold drawn music wire specimens failed well below the 230,000 psi. yield strength although one test plotted off the graph at 221,000 psi.

Negative correlation is also indicated for rich mortar as illustrated by Figure 31. Although the 1.72% galvanized and the 0.96% music wire specimens were additionally subjected to bending.

TABLE 3

Wire Stresses at Failure of Lean Mortar*

	Wire Type	Spacing (inches)	Vol % Wire	Wire Stress: Initial Stable Cracking	Wire Stress: Crack 100% W.
Single Layer	Stainless Steel	0.08	1.03	** 34,700	-
		0.10	1.11	57,000	71,000
		0.12	0.89	42,500	61,900
	Music Wire	0.08	0.85	67,600	92,000
		0.10	0.90	** 40,000	-
		0.12	1.04	78,400	160,000
Double Layer	Stainless Steel	0.08	1.42	38,900	58,300
		0.10	1.11	*** -	57,500
		0.12	0.95	39,800	67,100
	Galvanized	0.08	1.28	28,000	42,200
		0.10	1.35	29,600	43,800
	Music Wire	0.08	1.15	67,000	221,000
		0.10	1.37	*** -	73,000
		0.12	1.04	50,900	67,100
Chopped	Stainless	0.117	2	49,300	-
	Galvanized	0.117	2.7	20,700	-
	Music Wire	0.117	2	53,100	113,000

*Assumes that wire carries entire load at this stress.
**Fracture due to bumping specimen
***First crack propagated all across.

TABLE 4

Wire Stresses at Failure of Rich Mortar*

	Wire Type	Spacing (inches)	Vol % Wire	Wire Stress: Initial Stable Cracking	Wire Stress: Crack 100% W.
Double Layer	Stainless Steel	0.08	2.1	15,800	27,100
		0.10	1.9	22,900	42,400
	Galvanized	0.08	1.75	23,200	53,500
		0.10	1.72	***22,700	33,100
	Music Wire	0.08	0.96	***63,600	80,500
		0.10	1.05	** -	40,000
Chopped	Stainless Steel	0.117	2	38,100	17,400
	Galvanized	0.117	2.7	21,700	20,100
	Music Wire	0.117	2	53,000	43,200

*Assumes that wire carries entire load at this stress.
**First crack propagated all across.
***Subjected to lateral bending as well as tension.

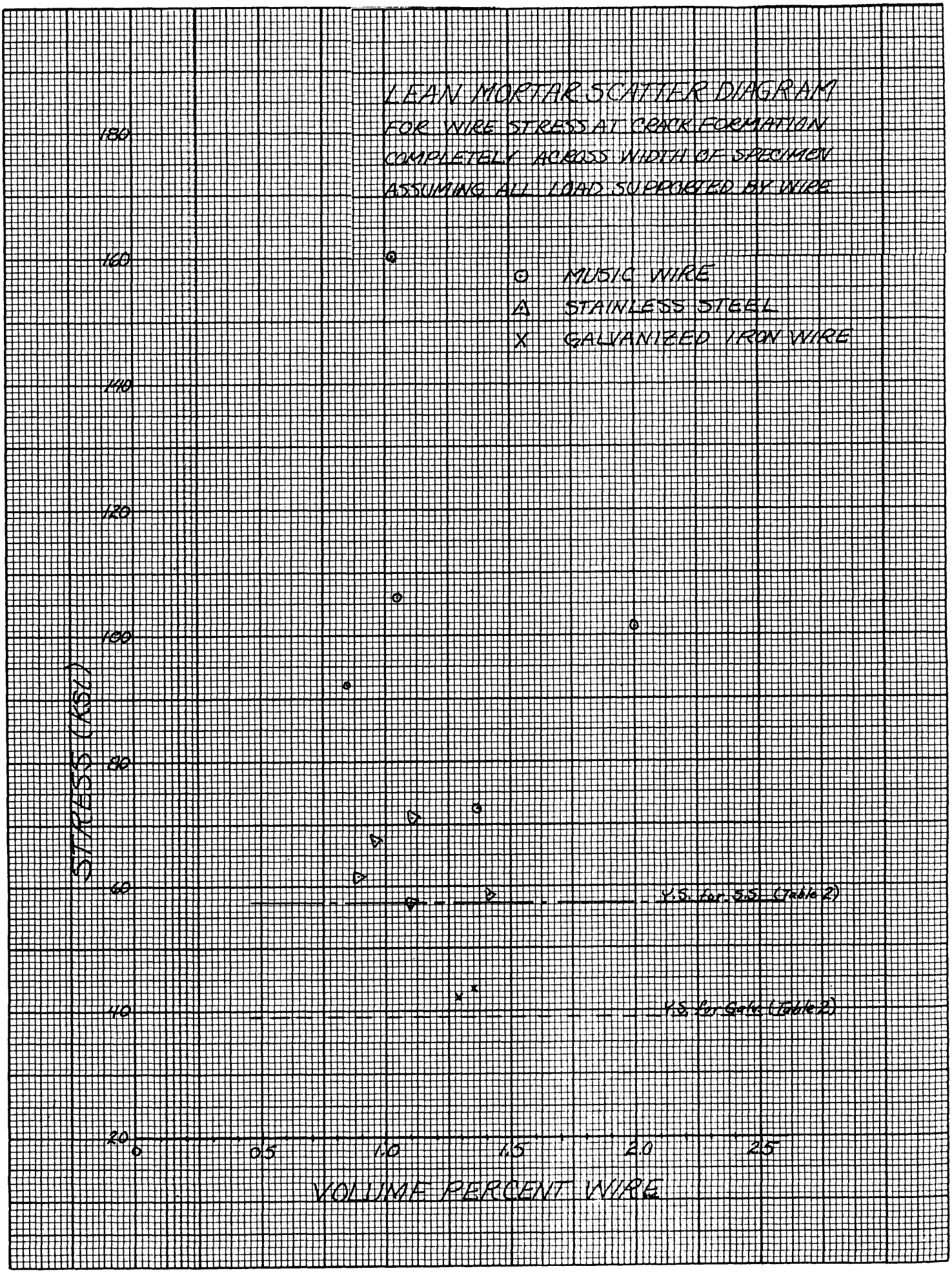

Figure 30

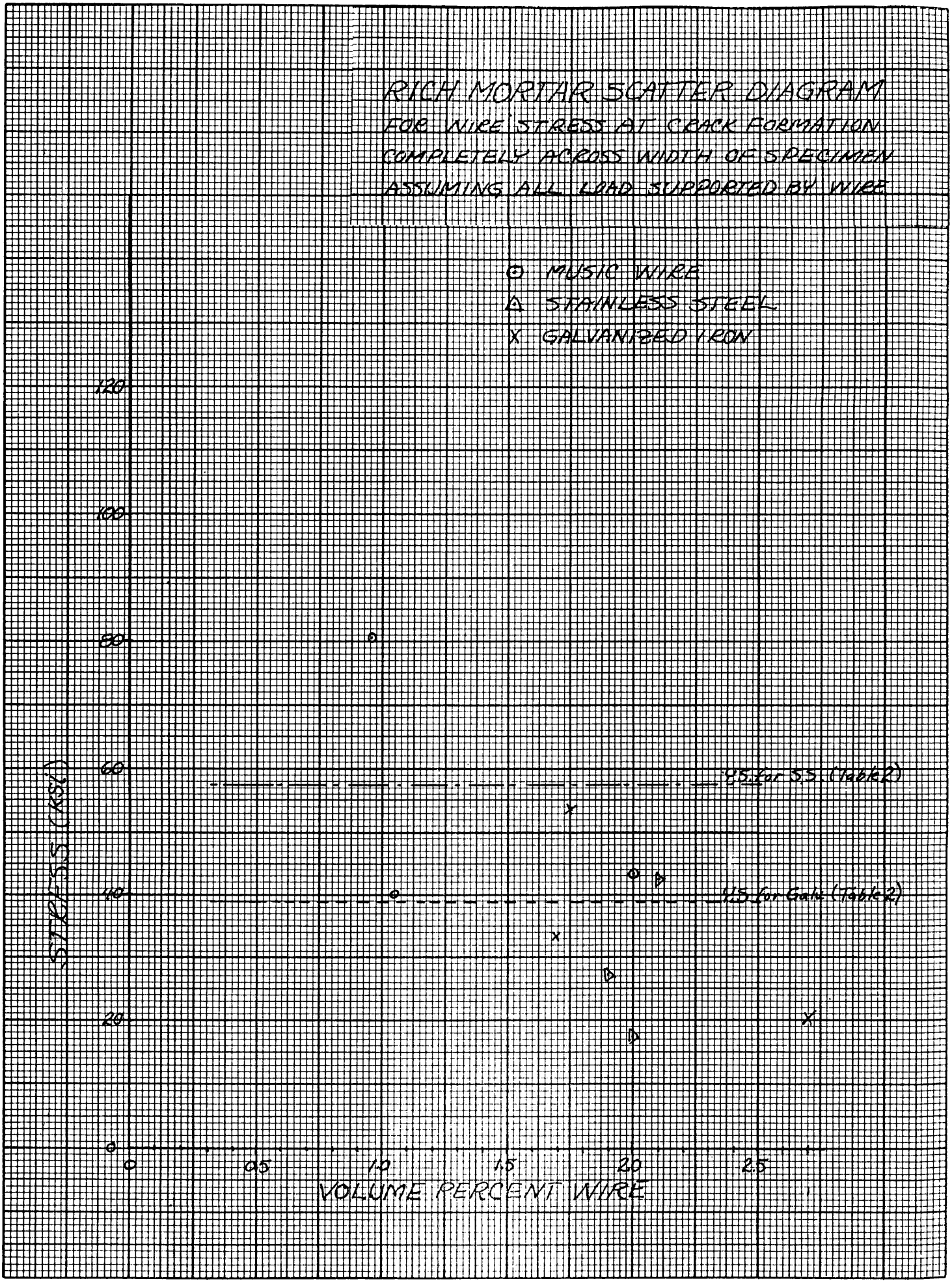

Figure 31

The rich mortar stainless steel specimens, however, are all well below the yield and pullout stresses measured on the Instron Testing Machine. Figure 16 still strongly suggests that pullout was occuring for the 1.9% SS specimen. There is too incomplete data available from this test series to allow pursuing further the possible correlation with yielding or pullout. The possibility certainly warrants further investigation.

5.3 Discussion of Photographs

The results contained in the photographs are by far the most valuable part of the thesis. As was stated in the procedure section, much redundancy resulted in photographs of crack formation and propagation behavior, thus the pictures in Figures 19 through 29 were selected because they best illustrate a point but the behavior illustrated may be considered representative of that recorded in the remainder of the approximately 200 pictures taken (38).

5.31 Crack Arrest Function of Wires

The evidence presented in Figure 19 together with that noted in paragraph B-1 of Appendix B prove that closely spaced wires do, in fact, cause crack arrest in a ferro-cement composite having good bonds. Even wires

which had been partially uncovered by the diamond saw exerted a strong arresting action as illustrated in Figure 19c and 19d. The technique of ruling pencil lines on the specimen surface at locations was suggested near the end of the test series. As a matter of fact, the suggestion was made just prior to the final straining increment on specimen 21 so that the crack arrest shown in Figure 19b was recorded coinciding with a free hand pencil line tracing the barely visible shadow of a wire just beneath the matrix surface. On the remaining parallel wire specimen, lines were ruled on both surfaces corresponding to the wire positions but the initial crack propagated completely across without stopping so that only the one picture was recorded of a crack being arrested by a wire fully covered by matrix material. Specimens 5, 10, and 13 exhibited this same behavior as described in Appendix B but pictures were not recorded of the crack tip stopping at a pencil line. Figure 19a illustrates the arrest action taking place in the direction of the specimen thickness.

5.32 Cracks Cross Wires in Perpendicular Direction

Figure 20 shows the tendency of wires to cross wires in a perpendicular direction. This behavior is easily explained by consideration of surface energy. The crack will always choose the path which expends the least surface energy (ie. that of the least resistance). If the bond at

the mortar wire interface is good, the path will always be perpendicular to the wire, then, since any other path would expend more surface energy.

5.33 Preferred Routes of Crack Travel

We have just discussed the fact that once started, a crack will choose the propagation path which expends the least energy. Figure 21 shows a few examples of these choices. In ascending order of elastic modulus and descending order of crack preference these regions are: voids and macroporous regions, existing cracks and microcracks in matrix and aggregate, microporous regions, aggregate interface, wire interfaces and the aggregate itself.

5.34 Crack Branching and Pairing

Chopped wire reinforced specimens show a much more erratic crack propagation path and much more marked tendency to branch into multiple cracks than do parallel wire specimens as illustrated by Figure 22a. It is believed that this is related to the preference of cracks to propagate past wires in a perpendicular direction. This is supported by the action of specimen 22 which was a poorly bonded chopped stainless steel specimen. It cracked straight across with little or no arresting action by the wires. Both front and back crack tips traveled together and deviated

around only aggregate.

Pairing also seems to be related to this preference of the crack to cross the wires in a perpendicular direction (See Figure 23). More pairing was noted in the well bonded parallel wire specimens and, in particular in the lean mortar music wire specimens. It is believed that the high modulus music wire pinches off cracks after a short distance of propagation. The great elastic strain energy is then further relieved by the initiation of another crack in the weakest region of matrix nearby (See Figure 24a). This second crack travels parallel to the first because of the tendency to cross wires in a perpendicular direction until it is somehow arrested.

In this way, cracks need not join up to cause a linked system of cracks completely across the specimen. At higher levels of stress, of course, they would be expected to begin propagating again since each crack tip constitutes a severe Griffith flaw.

5.35 Shrinkage Cracking and Microporosity

The rich mortar specimens were characterized by more microporosity and shrinkage cracking than were the lean mortar specimens as illustrated in Figure 24. This follows from the fact that the tendency for volume change in concrete from loss of moisture is almost entirely due to the effects on

the tobermorite gel crystals (39). This is believed to have been the principal reason for the low strength and unpredictable behavior of the rich mortar specimens. For example, specimen #18 failed at a much lower stress than did other rich mortar specimens. It was the only rich mix specimen which was allowed to cure under water for only 7 days followed by 7 days drying as had been done with all the lean mix specimens. All other rich mix specimens received a 14 day underwater cure.

5.36 Aggregate-Paste Interface Cracking

There was much evidence of aggregate-paste interface cracking, both on the specimen outer surfaces and in post straining sections taken from regions removed from the notch and fracture surface. Figure 25 shows a representative sampling of the cracks observed. It is significant to note that with the optical microscope the observer was unable to locate cracks which had propagated in those regions where parallel sections were taken. Such cracks were finally found in sections taken from specimen 13 by the scanning electron microscope. See Figure 21c and Figure 25a.

The stress levels in these regions averaged 80% of those in the notched region and it should be expected that many more of these cracks would have propagated. It is unfortunate that the scanning electron microscope was not

available for study of the other sections. By not having studied the other parallel sections with the SEM as well as with the Reichart Optical microscope, some doubt is cast upon the ability of the optical microscope to exactly fix the location of the crack tip as it propagated. The reader should be reassured, however, because once a crack was located with the optical microscope it could be tracked to its very tip by careful manipulation of the focus to keep the crack edges in focus. The principal limitation of the Reichart Optical microscope was in the search for crack initiation sites. For this reason the Zeiss stereoscopic microscope was used for these initial searches.

5.37 Cement Paste-Wire Bonding

Figure 26 illustrates the relative efficiencies of the bonds to each of the three wire surface types; specimens 13 and 27 are galvanized; specimens 22 and 23 are stainless steel, and specimen 17 is music wire. The bond to the galvanized wire is obviously the best, music wire is apparently next best and stainless steel is the least efficient as illustrated in Figure 26e. This relative ranking of bond efficiency is the same as that found in the pullout tests.

6.38 Air Bubble Attraction to Wires

Figure 27 clearly illustrates that air bubbles are

attracted to wires. This causes some problems since areas of weakness are concentrated near the reinforcing member so that a bridge around the wire is available to cracks. Further these regions are themselves crack initiation sites. See Figure 27d.

5.39 Cracks Parallel to Stress Field

Two causes were noted for the formation of cracks parallel to the stress field.

Specimen #21 was notched deeper than were most of the samples. As a result, one wire was cut in the region of Figures 28a through 28c. Thus, upon straining, these two half wire segments were not restrained from moving relative to their neighboring wires. A shearing force was developed and cracking occured on both sides of the notch.

Specimen 20 developed longitudinal cracks on both ends of a large void which uncovered the reinforcing wires on that side. The cracks developed in line with these uncovered wires - again indicating shearing action of the unrestrained wires.

5.40 Fracture Surface

Figure 29 illustrates the general disruption in the immediate vicinity of the fracture surface.

VI. CONCLUSIONS

1. There is a possible correlation of yielding of the wire reinforcement with the development of a crack completely across the width of a tension member.
2. Closely spaced wire reinforcement does, in fact, perform an arresting function so that tensile crack propagation takes place in a series of unstable increments which are pinched off or arrested as elastic energy is relieved.
3. Cracks cross wires in a perpendicular direction if the bond is good.
4. Members reinforced with chopped wires have more erratic crack propagation paths and often have multiple branching of cracks.
5. Members reinforced with parallel high strength cold drawn wires tend to develop the first complete crack by pairing rather than by a single crack.
6. Rich mortar tends to produce more shrinkage cracks and microporosity than does lean mortar.
7. Regions removed from the notch and fracture surface tend to form microcracks in the aggregate paste interfaces but not to propagate these cracks at 80% of the stresses causing failure at the notched region.

8. Wire bonds on all wires are sufficiently good that cracking of mortar occurs prior to pullout of the wires.
9. Bond efficiency of the three wire surfaces tested is in order of decreasing efficiency; galvanized, bright music wire, stainless steel.
10. Continuous parallel wires too near surface and broken or cut wires at any depth of cover can cause longitudinal cracking by a shearing action on the matrix.

VII. RECOMMENDATIONS

1. A series of tests should be conducted to determine if, in fact, the first complete crack across the member occurs at or above the yield stress of the wires.
2. When time permits, all Type I Portland cement specimens should be allowed to cure under water for at least 28 days so that all are at essentially their full strength when tested.
3. Design more reliable system for gripping specimens to insure that no lateral bending is introduced.

BIBLIOGRAPHY

1. Nervi, P.L., "Ferro-Cemento" in Structures, translated by Giuseppina and Maria Salvadori, 1956, F.W. Dodge Corp., New York, pp. 40-46.

2. Slayter, G., "Two Phase Materials", Scientific American vol. 206, No. 1, January 1962, p. 124.

3. Romualdi, J.P. and Batson, G.B.,"Behavior of Reinforced Concrete Beams with Closely Spaced Reinforcement", Journal of A.C.I., vol. 60, No. 40, June 1963, pp. 775-788.

4. Collins, J.F. and Claman, J.S., Ferro-Cement for Marine Application - An Engineering Evaluation, Paper presented before the New England Section of The Society of Naval Architects and Marine Engineers at Cambridge, Mass. on March 7, 1969.

5. Committee No. 207, Causes, Mechanisms and Control of Cracking in Concrete, Special Publication No. 20, 1966, American Concrete Institute, Pontiac, Mich.

6. Moavenzadeh, F., Szekessy, L., Bremner, T.W., Walkinshaw, J.L., "Fracture of Brittle Materials" in Quarterly Progress Report of the Inter American Program R 68 - 78, August 1968, Department of Civil Engineering, Massachusetts Institute of Technology, Cambridge, Mass. pp. 6-7.

7. Brunauer, S. and Copeland, L.C., "The Chemistry of Concrete", Scientific American, vol. 210, no. 4, pp. 81-87, April 1964.

8. Chatterji, S. and Jeffery, J.W., "Strength Development in Calcarious Cements", Nature, vol. 214, p. 559-561, 1967.

9. Philler, R.E., "The Origin of Strength of Concrete", Symposium on Structure of Portland Cement Paste and Concrete, Special Report No. 90, Highway Research Board, Washington, D.C., pp. 175-185, 1966.

10. Evans, R.H. and Kong, F.K., "The Extensibility and Microcracking of In-Situ Concrete in Composite Prestressed Beams", The Structural Engineer, vol. 24, no. 6, pp. 181-189, 1964.

11. Evans, R.H., "Extensibility and Modulus of Rupture of Concrete", Structural Engineer, vol. 2, no. 12, pp. 370-375, 1946.

12. Inglis, C.E., Transactions, Institute of Naval Architects, London, vol. 55, pp. 219, 1913.

13. Griffith, A.A., "The Phenomena of Rupture and Flaw in Solids:, Philosophical Transactions of The Royal Siciety of London, vol. 221, pp. 163-198, 1921.

14. Sack, R.A., Extension of Griffiths Theory of Rupture to Three Dimensions", The Proceedings of The Physical Society of London, vol. 58, part 6, pp. 729-736, 1946.

15. Irwin, G.R., "Fracture Dynamics", American Society for Metals, Transactions, vol. 40A, pp. 147-165, 1948.

16. Irwin, G.R. "Analysis of Stresses and Strains Near the End of a Crack Traversing a Plate", Journal of Applied Mechanics, vol. 24, pp. 361-364, 1957.

17. Orowan, E., "Energy Criterion of Fracture", Technical Report Number 3, Massachusetts Institute of Technology, July 1954.

18. Irwin, G.R., and Kies, J.A., "Fracturing and Fracture Dynamics", Welding Journal, vol. 31, pp. 955-100S, 1952.

19. Felbeck, D.K. and Orowan, E., "Experiments on Brittle Fracture of Steel Plates", Technical Report Number 1, Massachusetts Institute of Technology, Cambridge, Mass., July 1954.

20. Orowan, E., "The Condition of High Velocity Ductile Fracture", Technical Report Number 4, Massachusetts Institute of Technology, July 1954.

21. Pellini, W.S., Advances in Fracture Toughness Characteristics Procedures and in Quantitative Interpretations to Fracture Safe Design for Structural Steels, NRL Report 6713, Naval Research Laboratory, Washington, D.C., April 3, 1968.

22. Kaplan, M.F., "Crack Propagation and the Fracture of Concrete", Journal of the A.C.I. Proceedings, vol. 58, no. 28, pp. 591-610, 1961.

23. Winne, D.H. and Wundt, B.M., "Application of the Griffith-Irwin Theory of Crack Propagation to the Bursting Behavior of Discs, Including Analytical and Experimental Studies", Transactions of A.S.M.E., vol. 80, pp. 1643-1655, 1958.

24. Glucklich, Joseph, "Fracture of Plain Concrete", Journal of Engineering Mechanics Division, Proceedings A.S.C.E., vol. 89, no. EM6, pp. 127-138, 1963.

25. Hsu, T.T.C., Slate, S.O., Sturman, G.M., and Winter, G.A., "Microcracking of Plain Concrete and the Shape of the Stress-Strain Curve", Journal of A.C.I., vol. 60, no. 14, February 1963, pp. 209-222.

26. Moavenzadeh, F., Kuguel, R., and Lim, B.K., Fracture of Concrete, Department of Civil Engineering, Massachusetts Institute of Technology, Cambridge, Mass., March 15, 1968.

27. Nakayama, T., "Direct Measurement of Fracture Energies of Brittle Heterogeneous Materials", Journal of American Ceramic Society, vol. 48, no. 11, Nov. 1965, pp. 583-587.

28. Lott, G.L. and Kesler, C.E., "Crack Propagation in Plain Concrete," Urbana, University of Illinois, T.A.M. Report, No. 648, 1964.

29. Hsu, T.T.C. and Slate, F.O., "Tensile Bond Strength Between Aggregate and Cement Paste or Mortar", Journal of the A.C.I., vol. 60, no. 4, April 1963, pp. 465-487.

30. Shah, S.P., and Winter, G., "Inelastic Behavior and Fracture of Concrete" in Causes, Mechanisms and Control of Cracking in Concrete, Special Publication No. 20, 1966, American Concrete Institute, Pontiac, Michigan, pp. 73-85.

31. Romualdi, J.P. and Batson, G.B., "Mechanics of Crack Arrest in Concrete", Journal of the Engineering Mechanics Division, Proceedings of A.S.C.E., vol. 89, no. EM3, June 1963, pp. 147-167.

32. Westergaard, H.M., "Bearing Pressures and Cracks", Journal of Applied Mechanics, vol. 6, no. 2, 1939, pp. 49-53.

33. McKenny, J.L.,"Tensile Strength of Steel Fiber Reinforced Concrete", Unpublished Masters Thesis, Clarkson College of Technology, Potsdam, New York, May 1964.

34. Romualdi, J.P., and Mandel, J.A., "Tensile Strength of Concrete Affected by Uniformly Distributed and Closely Spaced Short Lengths of Wire Reinforcement", Journal of the A.C.I., vol. 61, no. 38, June 1964, pp. 657-672.

35. Romualdi, J.P., Ramey, M. and Sanday, S.C., "Prevention and Control of Cracking by Use of Short Random Fibers" in Causes, Mechanisms and Control of Cracking in Concrete, Special Publication No. 20, 1966, American Concrete Institute, Pontiac, Mich, pp. 179-202.

36. Collins, J.F., Tensile Strength of Mesh Reinforced Mortar", An unpublished team project for Course 1.46 at Massachusetts Institute of Technology, May 17, 1968.

37. Collins, J.F., "An Investigation into the Importance of bond Strength in Ferro Cement", An unpublished Naval Engineers Thesis Department of Naval Architecture and Marine Engineering, Massachusetts Institute of Technology, May 23, 1969.

38. Crow, H.E., "Crack Propagation and Arrest in Ferro-Cement." An unpublished term project for Course 1.46 at Massachusetts Institute of Technology, May 26, 1969.

39. Tazawa, E., Williamson, R.B. and McGarry, F.J., Influence of Curing Time on Shrinkage and Weight Loss of Hydrating Portland Cement, Department of Civil Engineering, Massachusetts Institute of Technology, Cambridge, Mass., December 1968.

APPENDIX A

Tables of Stress Strain Data

Specimen Number 1

One Layer 33 Gauge SS Wire at 0.08" Spacing in 0.4 C/S Mortar
Cross Section Area: 0.1095 in^2; Wire Area: 0.00113 in^2;
Volume % Wire: 1.03; Specimen Length: 5.2"

Strain Gauge μ-in/in	Load lbs.	Elongation in x 10^3	Stress psi	Strain in/in x 10^3	Remarks
3000	0	0	0	0	
3030	14.5	9	132	1.73	
3080	39	14	356	2.69	
3080	39	18	356	3.46	Crack started and traveled 0.7 width.

Accidentally bumped strain frame causing fracture of entire cross section.

Specimen Number 2

One Layer 33 Gauge SS Wire at 0.10" Spacing in 0.4 C/S Mortar
Cross Section Area: 0.092 in^2; Wire Area: 0.00102 in^2;
Volume % Wire: 1.11; Specimen Length: 5.22"

Strain Gauge μ-in/in	Load lbs.	Elongation in x 10^3	Stress psi	Strain in/in x 10^3	Remarks
3000	0	0	0	0	
3110	53	13	576	2.49	
3120	58	14	630	2.68	Cracked to 0.5 width.
3145	70	14.5	761	2.77	Crack moves again.
3150	72.5	15.5	789	2.96	Fracture all across.

Specimen Number 3

One Layer 33 Gauge SS Wire at 0.12" Spacing in 0.4 C/S Mortar
Cross Section Area: 0.101 in^2; Wire Area: 0.000904 in^2;
Volume % Wire: 0.89; Specimen Length: 5.21"

Strain Gauge μ-in/in	Load lbs.	Elongation in x 10^3	Stress psi	Strain in/in x 10^3	Remarks
3000	0	0	0	0	
3040	19.5	6	193	1.15	
3054	26	7	258	1.34	
3064	31	8	307	1.54	
3070	34	9	337	1.73	
3080	39	10	386	1.92	Crack started and traveled 0.3 width.
3095	46	11	456	2.11	
3126	61	12	604	2.3	Second crack started opened wide-100% width.
3130	63	13	624	2.5	
3140	68	14	673	2.7	First crack still moving.

Specimen Number 4

One Layer 33 Gauge Music Wire at 0.08" Spacing in 0.4 C/S Mortar
Cross Section Area: 0.133 in^2; Wire Area: 0.00113 in^2;
Volume % Wire: 0.85; Specimen Length: 5.17"

3000	0	0	0	0	
3050	24	8	180	1.55	
3082	39.5	10.5	296	2.03	
3103	50	12	376	2.32	
3122	59	13	444	2.52	
3136	65.5	14.5	492	2.8	
3155	75	16	563	3.1	
3158	76.5	17	575	3.29	
*3140	*67.5	17	*508	3.29	Crack started; stopped at 0.5 width.
3172	83	18	624	3.48	Fine 2nd crack appeared.
3186	90	18.5	676	3.58	
3198	96	19	721	3.67	
3210	102	19.5	767	3.77	
*3200	*96.5	19.5	*725	3.77	No apparent reason for stress relaxation.
3215	104	20	781	3.87	
*3205	*98	21	*736	4.07	Cracked all across.

*Stress relaxed due to formation of crack.

Specimen Number 5

One Layer 33 Gauge Music Wire at 0.10" Specing in 0.4 C/S Mortar
Cross Section Area: 0.113; Wire Area: 0.00102 in^2;
Specimen Length: 5.22"; Volume % Wire: 0.9

Strain Gauge u-in/in	Load lbs.	Elongation in x 10^3	Stress psi	Strain in/in x 10^3	Remarks
3000	0	0	0	0	
3020	9.6	2	85	0.38	
3040	12.3	4	171	0.77	
3050	24.2	5.5	214	1.05	
3054	26.1	6	231	1.15	
3062	39	7	266	1.34	
3084	40.6	9	360	1.73	
3090	43.5	11	385	2.11	Metallic Ping - Cracked all across top face.
3115	55.6	12	491	2.30	Crack only 0.45 width on back face
3130	62.8	13	556	2.30	
3150	72.4	14	640	2.68	Back crack moved about 0.1".
*3110	*53.1	14	470	2.68	Bumped strain frame and fracture completed all across.

*Stress relaxed due to formation of crack.

Specimen Number 6

One Layer 33 Gauge Music Wire at 0.12" Spacing in 0.14 C/S Mortar
Cross Section Area: 0.120 in^2; Wire Area: 0.0009;
Volume % Steel: 0.75; Specimen Length: 5.12"

3000	0	0	0	0	
3018	9	4	75	0.783	
3036	17.5	8.5	146	1.66	
3070	34	15	283	2.94	Grip slipped.
3086	43	21	358	4.11	
3110	53	23	442	4.5	
3147	71	25	591	4.89	Crack started, traveled 0.75 W.
3153	74.5	26	621	5.09	
3175	85	27	708	5.28	
3200	92	27.5	763	5.38	
3212	100	28	833	5.48	Crack moved again.
3220	107	28.5	892	5.57	
3235	113	29	941	5.68	
3250	121.5	30	1001	5.86	
3280	135.5	31	1130	6.06	
3300	145	32	1208	6.26	Fractured all the way.

Specimen Number 7

Two Layers 33 Gauge SS Wire at 0.08" Spacing in 0.4 C/S Mortar
Cross Section Area: 0.141 in^2; Wire Area: 0.00215 in^2;
Volume % Steel: 1.42; Specimen Length: 5.1"

Strain Gauge μ-in/in	Load lbs.	Elongation in x 10^3	Stress psi	Strain in/in x 10^3	Remarks
3000	0	0	0	0	
3030	15	4	106	0.784	
3050	24.5	9	174	1.77	
3074	36.5	12	249	2.36	
3090	42	13.5	298	2.65	
3136	65.5	17.5	464	3.43	
3142	68.5	19	486	3.73	
3157	76	21	538	4.12	
3170	82.5	23.5	584	4.62	
3173	83.5	24.5	592	4.81	Crack started.
3180	87.5	25	620	4.9	
3210	102	26	723	5.1	Crack moves again
3218	106	27.5	751	5.4	and stops.
3237	115	28	815	5.49	
3244	118	29	837	5.68	
3250	121	30	858	5.89	
3254	123	31	872	6.08	
3265	126	32	894	6.28	Crack started again Propagated all way.

Specimen Number 8

Two Layers 33 Gauge SS Wire at 0.10" Spacing in 0.4 C/S Mortar
Cross Section Area: 0.173 in^2; Wire Area: 0.001924 in^2;
Volume % Steel: 1.11; Specimen Length: 4.97"

3000	0	0	0	0	
3020	9.5	11	55	2.22	
3045	22	18	127	3.6	
3070	34	23	196	4.6	
3100	48	28	278	5.6	
*3100	*48	31	*278	6.2	Grip slipped.
3120	58	48	346	9.7	
3163	79	49	456	9.9	
3185	89.5	51	517	10.2	
3228	110	52	636	10.4	
*3200	*96.5	52.5	*558	10.6	Relaxed to 3200 after fracturing all the way across.

*Stress relaxed due to formation of crack.

Specimen Number 9

Two Layers 33 Gauge SS Wire at 0.12" Spacing in 0.4 C/S Mortar
Cross Section Area: 0.1785 in^2; Wire Area: 0.001695;
Volume % Wire: 0.95; Specimen Length: 5.17"

Strain Gauge μ-in/in	Load lbs.	Elongation in x 10^3	Stress psi	Strain in/in x 10^3	Remarks
3000	0	0	0	0	
3030	14.5	4	81	0.77	
3040	19.5	7	109	1.35	
3072	35	10	196	1.93	
3088	42.5	12	238	2.32	
3094	45	13	252	2.52	
3104	50	15	280	2.90	
3122	59	17	331	3.29	
3140	67.5	19	378	3.67	Stress relieved as
*3130	*62.5	19.5	*350	3.77	crack started -
3220	106	20.5	594	3.97	traveled 0.1 width.
3235	114	21.5	638	4.17	Crack opening.
*3185	*89.5	23	*502	4.44	Brittle fracture all across with

*Stress relaxed due to formation of crack. 2nd crack.

Specimen Number 10

Two Layer 33 Gauge Music Wire at 0.08 " Spacing in 0.4 C/S Mortar
Cross Section Area: 0.1874; Wire Area: 0.0215;
Volume % Wire: 1.15; Specimen Length: 5.07"

3000	0	0	0	0	
3060	29	3	155	0.58	
3100	48	5	256	0.98	
3134	65	6	347	1.19	
3150	72.5	7	387	1.38	
3198	95.5	8	510	1.58	
3220	106	8.5	566	1.68	
3250	121	9	646	1.78	
3274	132	10	705	1.97	
3298	144	10.5	769	2.07	Crack started, traveled
3320	155	10.5	828	2.07	0.5 W.
3340	164	11	875	2.17	
3365	176	11.5	940	2.27	Crack opened wide-0.7 W.
3410	198	12	1055	2.36	
3510	246	-	1315	-	Crack traveled all across.

Specimen Number 11

Two Layers 33 Gauge Music Wire at 0.10" Spacing in 0.4 C/S Mortar
Cross Section Area: 0.140 in^2; Wire Area: 0.00192 in^2;
Volume % Wire: 1.37; Specimen Length: 5.04"

Strain Gauge μ-in/in	Load lbs.	Elongation in x 10^3	Stress psi	Strain in/in x 10^3	Remarks
3000	0	0	0	0.0	
3047	22.5	4.5	161	0.883	
3078	38	6.5	272	1.29	
3118	53	9	378	1.79	
3175	85	12	607	2.38	
3244	118	16	842	3.18	
3284	138	18	985	3.57	
3288	140	19	1000	3.77	Brittle fracture all way across.

Specimen Number 12

Two Layers 33 Gauge Music Wire at 0.12" Spacing in 0.4 C/S Mortar
Cross Section Area: 0.163; Wire Area: 0.001695;
Volume % Wire: 1.04; Specimen Length: 5.17"

3000	0	0	0	0	
3034	16	3	98	0.58	
3050	24	4	147	0.77	
3094	45.5	9	280	1.74	
3110	53	11	325	2.13	
3122	59	13	362	2.51	
3145	70	15	430	2.9	
3164	79	16	485	3.1	
3180	87	17	533	3.29	Audible sound, crack 0.9W.
3200	96.5	18	592	3.48	
3220	106	18.5	650	3.58	
3235	114	19	700	3.68	Found 2nd crack all the way across.

Specimen Number 13

Two Layers 30 Gauge Galv. Iron Wire at 0.08" Spacing in 0.4 C/S Mortar
Cross Section Area: 0.168; Wire Area: 0.00215; Volume %
Wire: 1.28; Specimen Length: 5.24"

Strain Gauge μ-in/in	Load lbs.	Elongation in x 10^3	Stress psi	Strain in/in x 10^3	Remarks
3000	0	0	0	0	
3025	12	3	71.5	0.57	
3040	19	5	113	0.95	
3050	24	6	143	1.14	
3060	29	8	173	1.53	
*3055	*26.5	9	*157	1.72	
3065	31.5	11	188	2.1	
3080	38.5	17	229	3.24	
3095	46	18	274	3.44	
3110	53	19	316	3.63	
3125	60.5	20	360	3.82	
3154	74.5	21	444	4.0	
3170	82	22	486	4.2	Tiny crack started 0.2 W.
*3150	*72.5	23	*432	4.39	
3185	89.5	23.5	533	4.49	
3240	116	24.5	690	4.68	
3260	125.5	26	746	4.96	Open very wide-0.8 W.
*3210	*101.5	26	*600	4.96	
3250	121	27	720	5.15	
*3240	*116	28	*690	5.34	
*3240	*116	29.5	*690	5.63	
3245	118	31	703	5.82	Completes cracking W.

Specimen Number 14

Two Layers 30 Gauge Galv. at 0.10" Spacing in 0.4 C/S Mortar
Cross Section Area: 0.194 in^2; Wire Area: 0.00262;
Volume % Wire: 1.35; Specimen Length: 5.2"

Strain Gauge μ-in/in	Load lbs.	Elongation in x 10^3	Stress psi	Strain in/in x 10^3	Remarks
3000	0	0	0	0	
3035	16.9	5	87.6	0.96	
3048	23.2	7.5	119	1.44	
3060	29	9.5	150	1.83	Strong tendency to relax stress between increments of stress.
3065	31.4	11	162	2.11	
3080	38.6	12	199	2.31	
3105	50.8	14.5	262	2.79	
3120	58	16	299	3.08	
3145	70	17.5	361	3.36	
3160	77.4	19	399	3.75	Very fine crack starts- 0.3 width.
*3150	*72.4	19	*373	3.75	Relaxed to 373 psi before next strain.
3190	91.7	20	473	3.84	
3220	106	21	546	4.04	Crack moved about 0.1"to 0.4 width.
3238	115	22	583	4.23	Crack moved about 0.1" to 0.5 width.
*3205	* 99	22	*510	4.23	
*3115	* 55.6	22	*286	4.23	

Specimen Number 15

Two Layers 3[illegible] Gauge SS Wire at 0.08" Spacing in 0.7C/S Mortar
Cross Section Area: 0.102; Wire Area: 0.00215;
Volume % Steel: 2.1; Specimen Length: 4.97"

3000	0	0	0	0	
3038	18.3	5	178	1.01	
3062	29.9	8	293	1.61	
3070	33.8	9	331	1.81	Crack started- 0.45 width front face.
*3060	*29	9	*284	1.81	Back face no cracking.
3070	33.8	9.5	331	1.91	
3078	37.6	10	368	2.01	
3082	39.6	11	388	2.21	
3090	43.4	12	425	2.42	
3096	46.3	13	454	2.62	
3102	49.2	14	482	2.82	
*3092	*44.4	14	*435	2.82	Back now cracked 0.3 W.
3112	54.1	18	530	3.62	Front crack - 0.5 W.
3120	57.9	23	568	4.63	Crack all across both sides.

*Stress relaxed due to formation of crack.

Specimen Number 16

Two Layers 33 Gauge SS Wire at 0.10 Spacing in 0.7 C/S Mortar
Cross Section Area: 0.1015; Wire Area: 0.001924;
Volume % Steel: 1.9; Specimen Length: 5.27"

Strain Gauge μ-in/in	Load lbs.	Elongation in x 10^3	Stress psi	Strain in/in x 10^3	Remarks
3000	0	0	0	0	
3056	27	6.5	266	1.23	
3080	38.6	8	382	1.52	Crack started-0.3 W.
*3067	*32.4	8	319	1.52	Back face stopped at 0.2
3100	48.3	9	476	1.71	
3118	57	10	562	1.90	
3126	60.9	11	600	2.09	Back face crack pairs 2nd starts from shrinkage cracks, 0.1".
3136	65.6	13	645	2.47	
3140	67.6	14	666	2.66	
3145	70	15	690	2.85	
3150	72.3	16	713	3.04	Front crack moving 0.1".
3160	77.2	18	761	3.42	Front crack moving 0.1".
3168	81.1	19	800	3.61	Front crack moving 0.1".
3170	82	21	809	3.99	
3170	82	22	809	4.18	

Specimen Number 17

Two layers 33 Gauge Music Wire at 0.08" Spacing in 0.7 C/S Mortar
Cross Section Area: 0.225; Wire Area: 0.00215;
Volume % Wire: 0.96; Specimen Length: 5.13"

3000	0	0	0	0	
3040	12.3	2	86	0.39	
3065	31.4	4	139	0.78	
3100	48.3	6	215	1.17	
3134	64.8	8	288	1.56	Crack started-0.4 W fron and 0.2 W back.
*3110	*53.1	8	*236	1.56	
3150	72.5	9	322	1.76	
3170	82.1	9.5	365	1.85	Front crack - 0.5 width.
*3090	*43.5	10	*193	1.95	Crack opened wide all across.

Back face closed up - hence grips introduced bending.

*Stress relaxed due to formation of crack.

Specimen Number 18

Two Layers 33 Gauge Music Wire at 0.10" Spacing in 0.7 C/S Mortar
Cross Section Area: 0.132; Wire Area: 0.00192;
Volume % Wire: 1.46; Specimen Length: 5.12"

Strain Gauge u-in/in	Load lbs.	Elongation in x 10^3	Stress psi	Strain in/in x 10^3	Remarks
3000	0	0	0	0	
3020	9.7	1	73.5	0.19	Small noise and crack started, ran-0.6 width.
3040	19.5	2	148	0.39	
3050	24	2.5	182	0.48	Very slight opening but no movement.
*3050	*24	3	*182	0.59	Crack finally moved-stopped at 0.7 width.
3060	29	4	220	0.78	
*3060	29	4.5	*220	0.88	Crack traveled to 0.8 W.
*3060	29	5.5	*220	1.07	Metallic ringing pop and found crack all across in region removed from notch.

Specimen Number 19

Two Layers 33 Gauge Music Wire at 0.10" Spacing in 0.7 C/S Mortar
Cross Section Area: 0.1825; Wire Area: 0.00192;
Volume % Wire: 1.05; Specimen Length: 5.26"

3000	0	0	0	0	
3015	7.2	2	39.4	0.38	
3020	9.7	4	53.2	0.76	
3030	14.5	5	79.3	0.95	
*3020	* 9.7	6	* 53.2	1.14	
3024	11.6	7	63.5	1.33	
3030	14.5	8	79.4	1.52	
3035	16.9	10	92.5	1.9	
3040	19.3	11	106	2.09	
3045	21.8	13	119	2.47	
3060	29	15	159	2.85	
3080	38.6	17	212	3.23	
3105	50.8	19	278	3.61	
3145	70.1	21	384	4.0	
3160	77.3	22	423	4.19	Loud pop - Cracked all across on both sides.
*3070	*33.8	22	*180	4.19	

*Stress relaxed due to formation of crack.

Specimen Number 20

Two Layers 30 Gauge Galv. Wire at 0.08" Spacing in 0.7 C/S Mortar
Cross Section Area: 0.167 in^2; Wire Area: 0.00293 in^2;
Volume % Wire: 1.75; Specimen Length: 5.08"

Strain Gauge u-in/in	Load lbs.	Elongation in x 10^3	Stress psi	Strain in/in x 10^3	Remarks
3000	0	0	0	0	
3020	9.6	3	57.4	0.59	
3040	19.3	7.5	115.5	1.48	
3058	28	10	168	1.97	
3072	34.8	12	209	2.36	
3080	38.7	13.5	231	2.66	
3090	43.5	14.5	266	2.85	
3104	50.2	16	301	3.15	Crack starts - 0.2 W.
3120	58	17	347	3.35	Another 0.3" long crack parallel to wire at about
3130	62.8	18	376	3.54	0.4 W. on back face.
3150	72.5	19	434	3.74	
3176	85	19.5	509	3.84	Parallel cracks from void on front face.
*3150	*72.5	21	*376	4.13	Crack moved to 0.85 W.
3180	87	23	521	4.53	
*3160	*77.2	23	*463	4.53	Stress relieving.
3196	94.6	24	566	4.72	
3210	101.5	25	607	4.81	
3222	107	26	641	5.11	
3238	115	28	689	5.51	Fracture all across.

Specimen Number 21

Two Layers 30 Gauge Galv. at 0.10" Spacing in 0.7 C/S Mortar
Cross Section Area: 0.153 in^2; Wire Area: 0.00262 in^2;
Volume % Wire: 1.72; Specimen Length: 5.17"

3000	0	0	0	0	
3025	12.1	2	79	0.39	
3040	19.3	4	126	0.77	
3060	29	7	190	1.36	
3075	36.2	8.5	236	1.65	
3090	43.4	10	284	1.93	
3102	49.2	11	322	2.13	
3112	54.1	12	354	2.32	
3124	59.8	13	392	2.51	
*3110	*53.1	13	*347	2.51	Crack started-0.4 W.
3124	59.8	14	392	2.71	
3168	81.1	15	530	2.90	
3180	86.9	16	568	3.10	Front crack all across,
*3094	*45.4	16	*297	3.10	Back at 0.1 W.
3110	53.1	16.5	347	3.19	
3130	62.7	17	410	3.29	Back crack-0.7W.

Grips had put lateral bending on specimen.

*Stress relaxed due to formation of crack.

Specimen Number 22

Two Volume % Chopped SS in 0.4 C/S Mortar
Cross Section Area: 0.237 in^2; Specimen Length: 5.23"

Strain Gauge u-in/in	Load lbs.	Elongation in x 10^3	Stress psi	Strain in/in x 10^3	Remarks
3000	0	0	0	0	
3040	19.3	8.5	81.5	1.63	
3065	31.4	10	132	1.91	
3080	38.7	12	163	2.3	
3115	55.6	15	234	2.87	
3145	70.1	17	296	3.25	
3200	96.7	20	408	3.83	Large crack opens - 0.85
*3140	*67.7	20	*287	3.83	width on both front-back.
3165	79.7	22	337	4.21	

Specimen Number 23

Two Volume % Chopped SS in 0.7 C/S Mortar
Cross Section Area: 0.198 in^2; Specimen Length: 5.12"

3000	0	0	0	0	
3077	37.2	4.5	188	0.88	
3104	50.2	5.5	254	1.07	
3118	57	6.5	286	1.27	
3134	64.7	7	327	1.37	
3158	76.3	8	385	1.56	
3175	84.4	9	426	1.76	
*3060	*29	9	*146	1.76	Cracked wide - 0.95 width on both sides.
3080	38.6	11	195	2.15	Crack all across.

Specimen Number 24

Two Volume % Chopped Music Wire in 0.4 C/S Mortar
Cross Section Area: 0.218; Specimen Length: 5.24"

3000	0	0	0	0	
3030	14.5	3	66	0.57	
3045	21.8	4.5	100	0.86	
3050	23.2	6	106	1.14	
3062	30	7.5	138	1.43	
3074	35.8	9.5	164	1.81	
3080	38.6	10	177	1.91	
3098	47.3	12	217	2.29	
3114	55	13.5	253	2.58	
3130	62.9	14.5	288	2.77	
3150	72.5	15.5	332	2.96	
3174	84	16.5	385	3.15	Relaxing stress between
3198	95.7	18	438	3.34	increments.

Specimen Number 24 (Cont'd)

Strain Gauge u-in/in	Load lbs.	Elongation in x 10^3	Stress psi	Strain in/in x 10^3	Remarks
*3154	74.7	18	*343	3.34	Very fine crack started- 0.45 width.
3210	101.5	19.5	465	3.72	
3250	121.0	21	555	4.01	
3260	126	22	578	4.2	
3300	145	23	665	4.39	
3340	164.5	24	755	4.58	
3350	169	25	775	4.77	
3390	188.5	26	865	4.96	Cracked all across back face.
*3345	* 167	26	*765	4.96	
3420	203	28	930	5.34	Front crack moves to 0.7W
*3380	* 183	28	*840	5.34	
3420	203	30	930	5.72	Cracked all across in several branches.

Specimen Number 25

Two Volume % Chopped Music Wire in 0.7 C/S Mortar
Cross Section Area: 0.210 in^2; Specimen Length: 5.20"

3000	0	0	0	0	
3020	9.7	7	46.2	1.35	
3026	12.5	10	59.5	1.92	
3050	24.2	13	115	2.5	
3062	30	15	143	2.88	
3086	41.6	16.5	197	3.17	
3110	53.1	18	253	3.46	
3134	64.6	20	308	3.85	
3158	76.3	21	363	4.04	
3170	82.1	23	390	4.33	
3180	87	24	414	4.61	
3190	91.7	25	437	4.81	Cracked - 0.9 W Front.
*3110	*53.1	25	*253	4.81	All across back.
3135	65.1	27	310	5.20	
3155	74.8	28	356	5.39	Crack all across both sides.

Specimen Number 26

2.7 Volume % Chopped Galv. Wire in 0.4 C/S Mortar
Cross Section Area: 0.23 in^2; Specimen Length: 5.26"

Strain Gauge u-in/in	Load lbs.	Elongation in x 10^3	Stress psi	Strain in/in x 10^3	Remarks
3000	0	0	0	0	
3010	4.8	2.5	20.9	0.43	
3020	9.7	5	42.3	0.95	
3027	13	8.5	56.6	1.61	
3042	20.3	11.5	88	2.19	
3050	24.1	13.5	105	2.57	
3060	29	15	126	2.85	
3070	33.8	16	147	3.04	
3082	39.5	18	172	3.42	
3094	45.4	20	198	3.8	
3100	48.3	20.5	210	3.9	
3110	53.2	21	231	4.0	— Crack opened wide all
*3030	*14.5	21	* 63	4.0	all across front.
3050	24.1	21.5	105	4.1	Stopped at 0.6 width
3060	29	22.5	126	4.28	on back.
3070	33.8	28.5	147	5.43	Back crack - 0.8 width.
					Back crack - 0.85 width.

Specimen Number 27

2.7 Volume % Chopped Galv. Wire in 0.7 C/S Mortar
Cross Section Area: 0.204 in^2; Specimen Length: 5.18"

3000	0	0	0	0	
3030	14.5	3	71	0.57	
3050	24.1	5	118	0.97	
3065	31.4	6	154	1.16	
3075	36.2	6.5	177	1.25	
3085	41	7	201	1.35	
3100	48.3	8	237	1.55	
3110	53.1	8.5	260	1.64	
3120	57.9	9	284	1.74	
3140	67.6	10	331	1.93	Audible pop; crack -
3150	72.4	11	355	2.12	0.95 W. front and
*3070	*33.8	11	*166	2.12	0.9 W. on back.
3095	45.9	11.5	225	2.22	
*3095	*45.9	12	*225	2.32	All across on front.
3095	*45.9	32	*225	6.18	All across on back.

*Stress relaxed due to formation of crack.

APPENDIX B

B-1 Narrative Descriptions of Failure

Certain specimens exhibited behavior which can be better understood if described with a narrative of how cracks initiated, were arrested and any unusual occurences that were noted as specimens were strained to failure.

B-2 Specimen 5 (One layer of 33 gauge music wire at 0.08 inches spacing in lean mortar).

A large crack popped open from the root of the notch accompanied by a metallic ping sound at a stress level of 385 psi. This crack traveled all the way across the top surface but was found to have been arrested at about 45% of width on the back surface. The back crack moved approximately 0.1 inches upon stressing to 640 psi., then fractured all the way across when the straining device was accidentally bumped. This specimen was unique among the single layer specimens in that the crack did not propagate across the same distance on front and back surfaces during each increment of straining. No bending was evident even after fracture but the layer of wires was much closer to the surface where arrest took place (See Figure 19a)

B-3 Specimen 10 (Two layers 33 gauge music wire at 0.08 inches in lean mortar).

A very fine crack initiated from the notch at about 780 psi. and traveled half way across the specimen. The back surface of this specimen was not inspected, again, because the differential cracking between front and back had not yet been noted.

This region of the crack opened wide with a stress of about 1000 psi., and the crack traveled to about 70% of the width. After each crack movement, the stress relaxed sharply. The crack then moved about 0.1 inches as stress was raised to 1055 and another 0.1 inches as stress was raised to 1265. The crack then appeared to close slightly so stress was raised to 1315 psi., causing the crack to continue all the way across (See Figure 13).

B-4 Specimen 13 (Two layers of 30 gauge galvanized wire at 0.08 inches spacing in lean mortar).

A tiny crack started from the notch at 486 psi. stress and stopped at 8 to 10% of width. A second crack was visible near the end of the first but there was no apparent link. After stressing to 533 psi. these two cracks joined and the total crack length was 25% of width. This region of the crack opened wide at a stress of 746 psi. and the crack tip traveled

to 80% of width, as the stress relaxed to 690 psi. Crack movement then began at less than 0.1 inches per straining increment. The maximum sustainable stress was 690 psi. The back surface was not inspected on this specimen. It had not yet been noticed that cracks were not propagating equally on both surfaces. No obvious bending was noted. Therefore, it is unlikely that a strong compression field was hiding a crack on the front surface. Straining was continued for another 0.004 inches elongation before the crack finished crossing the specimen (See Figure 13).

B-5 Specimen 17 (Two layers of 33 gauge music wire at 0.08 inch spacing in rich mortar).

This rich mortar specimen is characterized by segregation and porosity on microscopic level, though fewer large voids are evident than in lean mortar.

The crack started from the notch at a relatively low stress level of 288 psi. In all cases, stress relaxed sharply after crack movement. This crack traveled 40% of width on front surface and 20% of width on back surface. The front crack moved about 0.1 inches at stress of 365 psi.; the back crack did not move. The front crack popped, opened and traveled all the way across at 375 psi. and the back crack closed tightly so that it was barely visible at 220X. The specimen was bowed up noticeably in the center. It was obvious that the grips were exerting lateral bending. After approximately five minutes,

the stress had relieved to 64 psi. and the specimen was restressed until the back crack propagated completely across. It became visible again at 365 psi. Apparently it was there all the time, but had been hidden by the compression field due to bending (See Figure 14).

B-6 Specimen 18 (Two layers of 33 gauge music wire at 0.10 inches spacing in rich mortar).

The crack initiated with an audible pop at the very low stress level of 73 psi. and traveled 60% of width. Stress was raised to 182 psi. at which level the crack appeared to be opening near its tip (although it did not move). The crack finally moved to 70% of width when the stress was raised again to 200 psi., then the stress relaxed to 182 psi. As stress was raised to 220 psi., there was a metallic ring again although the main crack didn't move. It was later found that a new crack had formed in a region removed from the notch. Straining was continued until the main crack propagated completely across at 0.013 inches additional elongation with a maximum sustained stress of 220 psi. Examination showed three cracks across specimen in regions removed from the notch.

B-7 Specimen 20 (Two layers of 30 gauge galvanized wire at 0.08 inches spacing in rich mortar).

The initial crack started at stress level 300 psi. This crack was 0.2 inches in front of the notch, running 0.3 inches

in a direction parallel to the wires. The crack on the back surface was perpendicular to the wires and 20% of width. Upon stressing to 509 psi., the back crack propagated to 85% of width and two cracks parallel to the stress field appeared on front surface. One crack came out of each side of a large void located 40% across width. The void dimensions were 0.2" diameter x 0.050" deep (See Figure 28). At 521 psi., something caused the stress to drop off rapidly to 463 psi., but it was not discovered what. Perhaps a small crack started in a region removed from the notch. Both cracks propagated completely across at 689 psi (See Figure 14).

B-8 Specimen 21 (Two layers of 30 gauge galvanized wire at 0.10 inches spacing in rich mortar).

The crack initiated from the side of the notch at 350 psi. and traveled away from the notch at a 45° angle to the wires to 10% of width where it apparently met another wire and changed directions perpendicular to wires. The crack stopped at 40% of width. A short crack started from the corresponding position on the opposite side of the notch and stopped after about 0.050" running parallel to wires. The notch cut through the wires here (See Figure 28). When stress was raised to 568 psi., the front crack traveled all across, but the back crack remained at 10% of width. The specimen was noticeably bent at this position so some lateral bending was exerted by the grips. Prior to applying more stress to this specimen, a pencil

mark was drawn marking the position of the next wire to be met by a propagating crack. Fortunately, it was possible to take a picture of the crack being arrested at this point on the next straining increment (See Figure 19). This crack initiated with 410 psi. and stopped at 70% of width as marked by the pencil.

B-9 Specimen 22 (Two volume % chopped stainless steel wire in lean mortar).

A large crack initiated from the notch at 410 psi. and traveled to 85% of width on both front and back surfaces. In contrast with crack in other chopped wire specimens, this crack was very straight with only the small deviations around aggregate particles. Very poor bonding with wire in this specimen (See Figure 26e).

The crack finished propagating completely across with a stress of 195 psi (See Figure 17).

B-10 Specimen 24 (Two volume % chopped music wire in lean mortar).

A very narrow crack initiated from the notch at 438 psi. and traveled 45% of width. At 865 psi. the back surface cracked completely across while the front crack remained at 45% of width. The back crack had two major branches, each of which again split into smaller branches (See Figure 22a).

Cracks in this specimen followed very circuitous paths by comparison with parallel wire specimens or specimen 22. At 765 psi., the front crack propagated to 70% of width. Stress was raised to 930 psi. where the crack moved 0.1 inches and the stress relaxed to 840 psi. The crack moved again and finally crossed the specimen.